The Cryosphere, 11, 407–426, 2017
www.the-cryosphere.net/11/407/2017/
doi:10.5194/tc-11-407-2017

The Cryosphere Open Access EGU

Spatial variability in mass loss of glaciers in the Everest region, central Himalayas, between 2000 and 2015

Owen King[1], **Duncan J. Quincey**[1], **Jonathan L. Carrivick**[1], **and Ann V. Rowan**[2]

[1]School of Geography and water@leeds, University of Leeds, Leeds, LS2 9JT, UK
[2]Department of Geography, University of Sheffield, Sheffield, S10 2TN, UK

Correspondence to: Owen King (gy08ok@leeds.ac.uk)

Received: 25 April 2016 – Published in The Cryosphere Discuss.: 23 May 2016
Revised: 27 December 2016 – Accepted: 9 January 2017 – Published: 3 February 2017

Abstract. Region-wide averaging of Himalayan glacier mass change has masked any catchment or glacier-scale variability in glacier recession; thus the role of a number of glaciological processes in glacier wastage remains poorly understood. In this study, we quantify mass loss rates over the period 2000–2015 for 32 glaciers across the Everest region and assess how future ice loss is likely to differ depending on glacier hypsometry. The mean mass balance of all 32 glaciers in our sample was -0.52 ± 0.22 m water equivalent (w.e.) a^{-1}. The mean mass balance of nine lacustrine-terminating glaciers (-0.70 ± 0.26 m w.e. a^{-1}) was 32 % more negative than land-terminating, debris-covered glaciers (-0.53 ± 0.21 m w.e. a^{-1}). The mass balance of lacustrine-terminating glaciers is highly variable (-0.45 ± 0.13 to -0.91 ± 0.22 m w.e. a^{-1}), perhaps reflecting glacial lakes at different stages of development. To assess the importance of hypsometry on glacier response to future temperature increases, we calculated current (Dudh Koshi – 0.41, Tama Koshi – 0.43, Pumqu – 0.37) and prospective future glacier accumulation area Ratios (AARs). IPCC AR5 RCP 4.5 warming (0.9–2.3 °C by 2100) could reduce AARs to 0.29 or 0.08 in the Tama Koshi catchment, 0.27 or 0.17 in the Dudh Koshi catchment and 0.29 or 0.18 in the Pumqu catchment. Our results suggest that glacial lake expansion across the Himalayas could expedite ice mass loss and the prediction of future contributions of glacial meltwater to river flow will be complicated by spatially variable glacier responses to climate change.

1 Introduction

Estimates of Himalayan glacier ice volume range from 2300 to 7200 km^3 (Frey et al., 2014 and references within) distributed among more than 54 000 glaciers across the Hindu Kush Himalayas and the Karakoram (Bajracharya et al., 2015). The current mass balance of Himalayan glaciers is predominantly negative, with accelerating mass loss having been observed over the past few decades (Bolch et al., 2012; Thakuri et al., 2014). This mass loss is occurring because of a combination of processes. Shrestha et al. (1999) show a rise in the mean annual air temperature of 0.057 °C a^{-1} across the Himalayas between 1971 and 1994. Bollasina et al. (2011) show a reduction in total precipitation (-0.95 mm day^{-1}) amounting to 9 to 11 % of total monsoon rainfall over a broad area of northern India between 1950 and 1999. Bhutiyana et al. (2010) show both decreasing total precipitation and a changing precipitation phase, with a lower proportion of precipitation falling as snow across the north-western Himalayas between 1996 and 2005. The snow cover season has been shortening as a result (Pepin et al., 2015). Under different climate scenarios, glacier imbalance in the region may contribute 8.7–17.6 mm of sea-level rise by 2100 (Huss and Hock, 2015). Prolonged mass loss from Himalayan glaciers may cause diminishing discharge of the largest river systems originating in the region (Immerzeel et al., 2010; Lutz et al., 2013), thereby impacting on Asian water resources in the long term.

Recent studies have identified spatial heterogeneity in mass loss across the Himalayas in the first decade of the 21st century (Kääb et al., 2012, 2015; Gardelle et al., 2013). Glaciers in the Spiti Lahaul and Hindu Kush are losing

mass most quickly (Kääb et al., 2015). Glaciers in the central Himalayas appear to have less negative mass balances (Gardelle et al., 2013). The anomalous balanced, or even slightly positive, glacier mass budget in the Karakoram is well documented (Bolch et al., 2012; Gardelle et al., 2012). Few previous studies have assessed the variability of glacier mass loss within catchments (Pellicciotti et al., 2015). Nuimura et al. (2012) examined the altitudinal distribution of glacier surface elevation change in the Khumbu region, Nepal and found similar surface-lowering rates over debris-free and debris-covered glacier surfaces. Gardelle et al. (2013) detected enhanced thinning rates on lacustrine-terminating glaciers in Bhutan, western Nepal and the Everest region, but did not make an explicit comparison with land-terminating glacier recession rates. Similarly, Basnett et al. (2013) have shown that lacustrine-terminating glaciers in Sikkim, in the eastern Indian Himalayas, experienced greater area loss between ~ 1990 and 2010 compared to land-terminating glaciers. Benn et al. (2012) have considered the role of glacial lakes in the wastage of debris-covered glaciers and proposed a conceptual model of Himalayan glacier recession that included important thresholds between regimes of ice dynamics and mass loss at different stages of lake development. Benn et al. (2012) suggest that an expansive, moraine dammed and potentially hazardous glacial lake may represent the end product of the wastage of a debris-covered glacier.

We aim to quantify glacier mass loss rates in three major catchments of the central Himalayas and assess the glacier-scale variability of ice loss within and between catchments. We specifically examine the mass balance, hypsometry and total area change of each glacier and compare those terminating in a glacial lake with those terminating on land. We use these data together with climatic data from the region to define the major mechanisms that may have driven mass loss in recent decades and to assess scenarios of likely future ice loss from our sample of glaciers.

2 Study area

We studied glaciers in three catchments of the Everest region (Fig. 1), spanning both Nepal and Tibet (China). Two of the catchments, the Dudh Koshi and the Tama Koshi, are located in north-eastern Nepal and drain the southern flank of the Himalayas. The third catchment is located to the north of the main orographic divide, and the glaciers drain north into Tibet (China). Most glaciers in the studied catchments are characterised by long (10–15 km) low-slope angled, debris-covered tongues that are flanked by large (tens of metres high) moraine ridges (Hambrey et al., 2008). Some glaciers have accumulation areas several kilometres wide that reach extreme altitudes (up to 8000 m in the case of the Western Cwm of Khumbu Glacier). Others sit beneath steep hillslopes (e.g. Lhotse and the Lhotse face), are fed almost exclusively by avalanches and are less than 1 km in width for their entire length.

The largest 40 of 278 glaciers in the Dudh Koshi catchment account for 70 % of the glacierised area (482 km^2 – Bajracharya and Mool, 2009). These glaciers are all partially debris-covered, with debris mantles reaching at least several decimetres in thickness (Rounce and McKinney, 2014; Rowan et al., 2015). Here, the total area of glacier surfaces covered by debris has increased since the 1960s (Thakuri et al., 2014) and several previous studies have published surface-lowering data for the catchment indicating accelerating surface-lowering rates over recent decades (e.g. Bolch et al., 2011; Nuimura et al., 2012). We select nine of the largest glaciers (Table S1 in the Supplement) for analysis, given that they provide the greatest potential volume of meltwater to downstream areas.

There are a total of 80 glaciers in the Tama Koshi catchment covering a total area of 110 km^2 (Bajracharya et al., 2015). We again selected the largest nine glaciers (Table S1) for analysis based on relative potential contributions to river flow. The Tama Koshi is a poorly studied catchment, perhaps best known for the existence of Tsho Rolpa glacial lake, which underwent partial remediation during the 1990s (Reynolds, 1999).

The 14 glaciers within our sample that flow onto the Tibetan Plateau (Table S1) all contribute meltwater to the Pumqu river catchment, which covers an area of 545 km^2 (Che et al., 2014). Debris cover is less prevalent on glaciers of the Pumqu catchment, and glacier recession has caused a 19 % of glacier area loss since 1970 (Jin et al., 2005; Che et al., 2014). There is relatively little information on glacier ELAs other than in the Dudh Koshi catchment. In the Dudh Koshi, Asahi (2001) estimated ELAs to be at around 5600 m a.s.l. in the early 2000s. Wagnon et al. (2013) measured annually variable ELAs of 5430–5800 m a.s.l. on the Mera and Polkalde glaciers between 2007 and 2012, Shea et al. (2015) estimate the current ELA to be 5500 m a.s.l., and Gardelle et al. (2013) estimated the ELA to be around 5840 m over the period 2000–2009. In the Pumqu catchment, those in the Rongbuk valley were estimated to be between 5800 and 6200 m a.s.l. for the period 1974–2006 (Ye et al., 2015).

A number of studies have identified an abundance of glacial water bodies in the Everest region. Salerno et al. (2012) identified 170 unconnected glacial lakes (4.28 km^2), 17 proglacial lakes (1.76 km^2) and 437 supraglacial lakes (1.39 km^2) in the Dudh Koshi catchment. Gardelle et al. (2011) identified 583 supraglacial ponds and lakes in an area comparable in coverage to Fig. 1. Watson et al. (2016) mapped 9340 supraglacial ponds onto eight glaciers of the Dudh Koshi catchment and Rongbuk glacier in the Pumqu catchment. Watson et al. (2016) also show a net increase in ponded area for six of their nine studied glaciers. Some of the largest glacial lakes in this region have also been expanding in recent decades (Sakai et al., 2000; Che et al., 2014; Somos-Valenzuela et al., 2014).

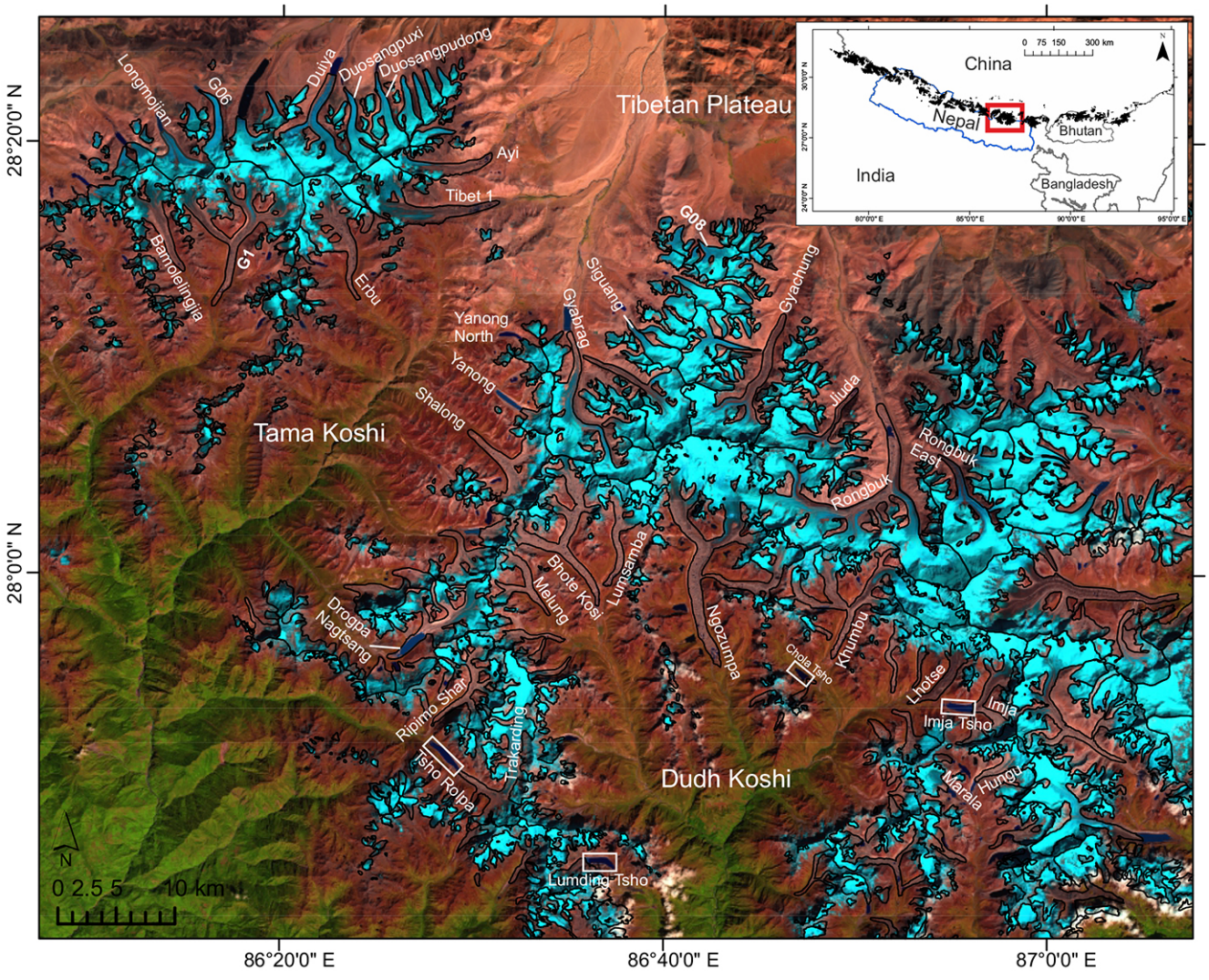

Figure 1. The glaciers of the Everest region. Named glaciers are the glaciers we highlight in this study. Major catchments include the Tama Koshi and Dudh Koshi on the southern flank of the Himalayas and the Pumqu river catchment on the northern side of the divide, with glaciers flowing onto the Tibetan Plateau (China). Named glacial lakes are highlighted, although many remain unnamed. Background imagery is a Landsat OLI image from 2014 available from http://earthexplorer.usgs.gov/.

This increased meltwater ponding at glacier termini has the potential to affect ice dynamics and down-valley meltwater and sediment fluxes (Carrivick and Tweed, 2013) as well as causing a hazard to populations living downstream. Several of the lakes have burst through their moraine dams in previous decades, causing rapid and extensive flooding downstream; the best studied outburst floods are those from Nare glacier in 1977 (Buchroithner et al., 1982) and from Dig Tsho in 1985 (Vuichard and Zimmerman, 1987).

We classify nine glaciers from the sample as lacustrine terminating, where the glacier termini and glacial lakes are actively linked. We do not consider either Rongbuk Glacier or Gyabrag Glacier as lacustrine terminating. Gyabrag Glacier is now separated from a large proglacial lake by a large outwash plain, and we do not believe the lake can have an influence on the retreat of the glacier. In the case of Rongbuk Glacier, the lake is supraglacial and far up-glacier from its terminal region and thus does not currently influence the recession of the terminus of the glacier. The expanding Spillway Lake at the terminus of Ngozumpa Glacier (Thompson et al., 2012) is currently of limited depth and is unlikely to affect glacier dynamics in its current state so we also exclude Ngozumpa Glacier from the lacustrine-terminating category.

Table 1. Scenes used in glacier outline delineation, ASTER DEM generation, SRTM ice facies mask generation and by the Polar Geospatial Center in the generation of SETSM DEMs.

Sensor	Scene ID	Date of acquisition	Purpose
Landsat OLI	LC81400412014334LGN00	30 Nov 2014	Glacier outlines
Landsat ETM+	LE71390412000302SGS00	29 Oct 2000	Glacier outlines
Landsat ETM+	LE71400402002005SGS00	5 Jan 2002	Ice facies mask
Landsat ETM+	LE71400412002005SGS00	5 Jan 2002	Ice facies mask
ASTER	L1A.003:2014050545	29 Nov 2014	ASTER DEM
WorldView 3	WV03_20150121_10400100076C0700	21 Jan 2015	SETSM DEM
WorldView 1	WV01_20150504_102001003C5FB900	4 May 2015	SETSM DEM
WorldView 1	WV01_20140115_102001002A289F00	15 Jan 2014	SETSM DEM
WorldView 1	WV01_20140324_102001002D263400	24 Mar 2014	SETSM DEM
WorldView 1	WV01_20150204_102001003A5B7900	4 Feb 2015	SETSM DEM
WorldView 2	WV02_20150202_103001003D4C7900	2 Feb 2015	SETSM DEM
WorldView 1	WV01_20140218_102001002C5FA100	18 Feb 2014	SETSM DEM
WorldView 1	WV01_20141022_102001003525D400	22 Oct 2014	SETSM DEM
WorldView 2	WV02_20141110_1030010039013C00	10 Nov 2014	SETSM DEM
WorldView 1	WV01_20141129_102001002776B500	29 Nov 2014	SETSM DEM
WorldView 1	WV01_20140514_102001003001E400	14 May 2014	SETSM DEM

3 Data sources and methods

3.1 Data sources

3.1.1 Digital elevation models

Our reference elevation dataset across all three catchments is the Shuttle Radar Topography Mission (hereafter SRTM) version 3.0, non-void-filled, 1 arcsec digital elevation model (hereafter DEM). The main objective of the SRTM mission was to obtain single-pass interferometric Synthetic Aperture Radar (SAR) imagery to be used for DEM generation on a near-global scale (56° S to 60° N – 80 % of the planet's surface) with targeted horizontal and vertical accuracies of 16 and 20 m, respectively, although Farr et al. (2007) report horizontal and vertical accuracies of better than 10 m for most regions globally. This dataset was acquired in February 2000 and was released at 30 m resolution in late 2014 (USGS, 2016). The SRTM data we used were acquired by a 5.6 cm C-band radar system.

Our 2014/2015 elevation dataset comprises a number of high-resolution (8 m grid) DEMs generated by Ohio State University and distributed online by the Polar Geospatial Center at the University of Minnesota that provide coverage of an extended area around the Everest region (Table 1). These stereo-photogrammetric DEMs have been generated using a Surface Extraction with TIN-based Search-space Minimization (hereafter SETSM) algorithm from WorldView 1, 2 and 3 imagery (Noh and Howat, 2015). The SETSM algorithm is designed to automatically extract a stereo-photogrammetric DEM from image pairs using only the Rational Polynomial Coefficients (RPCs) as geometric constraints. The geolocation accuracy of RPCs without ground control for WorldView 1 and 2 data is 5 m (Noh and Howat, 2015) which may ultimately result in matching failure. The SETSM algorithm updates RPCs to mitigate this error and produces DEMs with an accuracy of ±4 m in X, Y and Z directions (Noh and Howat, 2015). SETSM DEMs are gap filled using a natural neighbour interpolation; we removed these pixels before DEM differencing and calculating glacier mass balance.

Over two small areas of the Dudh Koshi (over the lower reaches of the Bhote Kosi and Melung glaciers), the SETSM DEMs contained data gaps. To complete coverage of DEMs over these glaciers we generated ASTER (Advanced Spaceborne Thermal Emission and Reflection Radiometer) DEMs and used the surface to cover elevation bands across the glaciers for which no data were available from the SETSM grids. We used ERDAS Imagine (2013) to generate ASTER DEMs with ground control points (GCPs) matched between features in the ASTER imagery and the high-resolution imagery available in Google Earth. We used a large number of GCPs (45) and tie points (>75) to minimise the root mean square error of GCP positions. All SETSM and ASTER DEMs were resampled to a 30 m resolution to match that of the SRTM data before any differencing was carried out.

3.1.2 Glacier outlines

Glacier outlines were downloaded from the Global Land Ice Measurements from Space Randolph Glacier Inventory (RGI) Version 5.0 (Arendt et al., 2015) and modified for 2000 and 2014 glacier extents based on Landsat scenes closely coinciding in acquisition with the DEM data. Glacier extents from these two epochs were used to calculate area changes. The 2000 Landsat scene was acquired by the Enhanced The-

matic Mapper Plus (ETM+) sensor and thus has a single 15 m resolution panchromatic band and six 30 m multispectral bands. The 2014 scene was acquired by the Operational Land Imager (OLI) sensor and has a single 15 m panchromatic band as well as eight 30 m multispectral bands. Both scenes were pan-sharpened to match the resolution of the multispectral bands to that of the panchromatic band before glacier outlines were adjusted. Adjustments were limited to correcting changes in glacier frontal position and changes along the lateral margins because of surface lowering.

3.2 DEM correction

3.2.1 Stereoscopic DEMs

We followed the three-step correction process of Nuth and Kääb (2011), through which biases inherent in stereoscopic DEMs can be corrected. We assessed and corrected where necessary for (i) a mismatch in the geolocation of the modern DEMs versus the reference SRTM dataset (in x, y and z direction), (ii) the existence of an elevation dependant bias and (iii) biases related to the acquisition geometry of the data. Each step was taken individually, so that separate error terms could be understood, rather than bundling them together as multiple-regression-based adjustments as previous studies have done, such as Racoviteanu et al. (2008) and Peduzzi et al. (2010). Corrections applied to DEMs for which any one of the three biases were present included shifting DEM corner coordinates, simple vertical shifting through addition or subtraction, and the fitting of linear and polynomial trends depending on the spatial variability of elevation differences across DEMs and through their elevation ranges. Acquisition of geometry-related biases (along or cross satellite track) were detected in two SETSM strips (Table 3) and both ASTER scenes and were corrected for using linear trends fitted through difference data. DEM coregistration was carried out following the conversion of SETSM elevation data to geoid heights using the Earth Gravitational Model (EGM) 2008 grid available from the National Geospatial-Intelligence Agency. Table 2 shows a summary of DEM difference data over stable, off-glacier areas before and after DEM coregistration.

3.2.2 SRTM DEM correction

Some studies have shown that the SRTM dataset may underestimate glacier surface elevations because of C-band radar wave penetration into snow and ice (Rignot et al., 2001). Kääb et al. (2012) assessed the magnitude of C-band penetration over various test sites in the Himalayas and over different ice facies (clean ice, snow and firn) by extrapolating ICESat vs. SRTM glacier elevation differences back to the SRTM acquisition date, showing penetration estimates of several metres. To account for this bias, we have corrected the SRTM dataset using the penetration estimates of Kääb et al. (2012), after generating a mask for clean ice, firn and snow cover using the most suitable Landsat ETM+ scenes (Table 1) available around the acquisition date of the SRTM dataset. We applied a correction to the SRTM DEM of +4.8 m over areas of firn/snow and +1.2 m over areas of clean ice (see Table S2 of Kääb et al., 2012). We do not apply any penetration correction over debris-covered areas given the uncertainty expressed by Kääb et al. (2012) about the influence of possibly greater than average snowpack depth at the point of ICESat acquisition and the properties of the snowpack at the point of SRTM data acquisition on their penetration estimate.

Berthier et al. (2006) suggested that the extreme topography present in mountain regions is poorly replicated in coarse-resolution DEMs such as the SRTM DEM. Different studies have applied positive or negative corrections to the SRTM DEM (Berthier et al., 2007; Larsen et al., 2007), depending on the severity of the terrain at their respective study sites. Inspection of DEM differences across the study site showed no clear relationship between elevation differences and altitude (see Fig. S1); thus no elevation-dependant correction was applied.

3.2.3 Gap filling and outlier filtering

Once DEMs had been co-registered and corrected for present biases, DEMs were differenced to yield surface elevation change data. To remove outlying values, we firstly excluded obviously incorrect difference values (exceeding ±120 m) and then followed the approach of Gardelle et al. (2013) in using the standard deviation of DEM difference data to classify probable outliers. We removed values exceeding 3 standard deviations. Such outlier definitions are justified in areas of shallow slope and high image contrast when DEM quality is generally high (Ragettli et al., 2016), but could be considered lenient where featureless surfaces, for example snow-covered areas of accumulation zones, might lead to poor elevation data derivation and limit the accuracy of stereoscopic DEMs. Noh and Howat (2015) show how the iterative approach of the SETSM algorithm and the high spatial and radiometric resolution of WorldView imagery preclude such an issue, and we therefore consider a 3 standard deviation threshold appropriate.

To complete data coverage and allow for glacier mass balance estimates, the filling of data gaps was required. Only small ($< \sim 5 \times 5$ grid cells) gaps were present in DEM difference data over most of the glaciers in our sample, but some larger gaps could be found over areas of steep surface slope, for example high in accumulation zones or where deep shadows might have been extensive in WorldView imagery. We filled gaps in DEM difference data using median values from the 100 m elevation band in which the data gap was situated (Ragettli et al., 2016).

Table 2. Mean differences and the standard deviation associated with off-glacier elevation difference data between ASTER, SETSM and SRTM DEMs before and after the DEM correction process. The uncertainty associated with DEM difference data (sum of standard error estimates for each 100 m elevation bin of difference data) is also listed for each SETSM and ASTER DEM.

Sensor	ASTER scene ID	Pre correction mean and SD stable ground differences Vs SRTM (m)		Post correction mean and SD stable ground differences Vs SRTM (m)		dh/dt uncertainty ($\pm$m a^{-1})
ASTER	L1A.003:2014050545	−64.12	25.99	0.43	11.30	0.47
	SETSM tile					
WV 3	WV03_20150121_10400100076C0700	−6.07	11.54	0.53	6.43	0.25
WV 1	WV01_20150504_102001003C5FB900	−5.68	15.76	−0.43	5.89	0.40
WV 1	WV01_20140115_102001002A289F00	−3.56	9.50	0.50	6.64	0.27
WV 1	WV01_20140324_102001002D263400	−2.21	8.92	0.07	5.90	0.33
WV 1	WV01_20150204_102001003A5B7900	−1.26	17.50	−0.36	5.65	0.31
WV 2	WV02_20150202_103001003D4C7900	−3.80	12.34	−0.03	6.56	0.29
WV 1	WV01_20140218_102001002C5FA100	−2.00	9.80	−0.23	6.71	0.28
WV 1	WV01_20141022_102001003525D400	−9.54	16.50	0.36	6.89	0.35
WV 2	WV02_20141110_1030010039013C00	−2.89	9.83	0.07	5.87	0.15
WV 1	WV01_20141129_102001002776B500	−5.72	8.31	0.16	4.76	0.18
WV 1	WV01_20140514_102001003001E400	−3.51	10.12	−0.26	5.91	0.26

3.3 Uncertainty

3.3.1 DEM differencing uncertainty

Our elevation change uncertainty estimates have been calculated through the derivation of the standard error ($E_{\Delta h}$) – the standard deviation of the mean elevation change – of 100 m altitudinal bands of elevation difference data (Gardelle et al., 2013; Ragettli et al., 2016):

$$E_{\Delta h} = \frac{\sigma_{\text{stable}}}{\sqrt{N}}, \quad (1)$$

where σ_{stable} is the standard deviation of the mean elevation change of stable, off-glacier terrain, and N is the effective number of observations (Bolch et al., 2011). N is calculated through the following:

$$N = \frac{N_{\text{tot}} \times \text{PS}}{2d}, \quad (2)$$

where N_{tot} is the total number of DEM difference data points, PS is the pixel size and d is the distance of spatial autocorrelation. We follow Bolch et al. (2011) in estimating d to equal 20 pixels (600 m). $E_{\Delta h}$ for each DEM is the sum of standard error estimates of each altitudinal band (Gardelle et al., 2013).

We have also considered whether the different acquisition dates of WorldView imagery (Table 1) have led to the sampling of seasonal glacier surface elevation variations caused by a remnant snowpack (e.g. Berthier et al., 2016). Such a bias should be partly corrected for during vertical DEM adjustment using off-glacier terrain assuming a similar snowpack thickness on and off-glacier (Wang and Kääb, 2015). Two overlapping SETSM DEMs (ending FA100 and 3C00 in Table 1) have been generated from WorldView imagery acquired before and after the summer monsoon (when glaciers receive most accumulation) of 2014; thus any spatially consistent vertical differences may show a remnant snowpack that would cause an elevation bias. The difference between these two SETSM DEMs over the Bamolelingjia and G1 glaciers is slight (mean 0.69 m, σ 3.81 m), but we cannot be sure that these differences represent a region-wide average. We have incorporated the mean elevation difference of these SETSM DEMs over glacier surfaces ($\text{d}Z_{\text{season}}$) into our overall uncertainty budget. We summed different sources of error quadratically to calculate our overall uncertainty ($\sigma_{\text{d}h/\text{d}t}$) associated with DEM difference data:

$$\sigma_{\frac{\text{d}h}{\text{d}t}} = \sqrt{E_{\Delta h}^2 + \text{d}Z_{\text{season}}^2}. \quad (3)$$

$\sigma_{\text{d}h/\text{d}t}$ is then weighted depending on the hypsometry of each glacier, giving a glacier-specific measure of elevation change uncertainty that considers the spatially non-uniform distribution of uncertainty (Ragettli et al., 2016).

3.3.2 Glacier area change uncertainty

There are two principal sources of uncertainty in the measurement accuracy of the position of a glacier margin: sensor resolution and the co-registration error between the images acquired at each measurement epoch (Ye et al., 2006; Thakuri et al., 2014). We follow the approach of Ye et al. (2006) to quantify the uncertainty associated with the total area changes documented across our sample of glaciers. We incorporate geolocation accuracy estimates of 10.5 m for Landsat ETM+ imagery and 6.6 m for Landsat OLI imagery (Storey et al., 2014) into the uncertainty budget and sug-

gest the total measurement uncertainty in glacier area between 2000 and 2015 image sets was $\pm 0.04\,\mathrm{km^2\,a^{-1}}$. Area-weighted, glacier-specific uncertainty estimates are given in Table S3.

3.4 Hypsometric analyses and elevation range normalisation

Glacier hypsometry, the distribution of a glacier area over altitude, is governed by valley shape, relief and ice-volume distribution (Jiskoot et al., 2009). It is important for the long-term glacier response because it defines the distribution of mass with elevation and thus determines how the glacier responds to changes in elevation-dependent temperature (Furbish and Andrews, 1984). To assess glacier hypsometry, we used the aforementioned glacier outlines and the SETSM DEMs, which offer better data coverage than the non-void-filled SRTM dataset, to split these glacier extents into segments covering 100 m elevation ranges, and calculated the area of each segment. We followed the approach of Jiskoot et al. (2009) to categorise each glacier or the population of glaciers in each catchment according to a hypsometric index (HI), where

$$\mathrm{HI} = \frac{(H_{\max} - H_{\mathrm{med}})}{(H_{\mathrm{med}} - H_{\min})} \tag{4}$$

and $H_{\max}$ and $H_{\min}$ are the maximum and minimum elevations of the glacier, and H_{med} is the median elevation that divides the glacier area in half (Jiskoot et al., 2009). Glaciers were grouped into five HI categories: 1 is HI < -1.5, very top heavy; 2 is HI -1.2 to -1.5, top heavy; 3 is HI -1.2 to 1.2, equidimensional; 4 is HI 1.2 to 1.5, bottom heavy; and 5 is HI > 1.5, very bottom heavy. Top-heavy glaciers store more ice at higher elevation, for example in broad accumulation zones, whereas bottom heavy glaciers have small accumulation zones and long tongues.

To construct elevation change and glacier hypsometry curves for the 32 glaciers in our sample, we have normalised the elevation range of each glacier following the method of Arendt et al. (2006):

$$H_{\mathrm{norm}} = \frac{(H - H_{\min})}{(H_{\max} - H_{\min})}, \tag{5}$$

where $H_{\min}$ and $H_{\max}$ are the elevations of the glacier terminus and the elevation maximum of each glacier. This normalisation process allows for a direct comparison of elevation changes and glacier hypsometry regardless of termini elevation. Surface elevation change and glacier hypsometry curves are presented in Figs. 5 and 6.

3.5 Mass loss calculations

A conversion factor of $850\,\mathrm{kg\,m^{-3}}$ was used to account for the density of glacier ice for all glaciers in the sample (Huss, 2013). We assigned an additional 7 % to mass loss uncertainty estimates to account for error in the density conversion (Huss, 2013). The mass loss estimates generated for lacustrine-terminating glaciers are slight underestimates because, with no information available on bed topography, we cannot account for ice that has been replaced by water during lake expansion. Mass balance estimates for these glaciers therefore only incorporate aerial mass loss from the 2000 calving front, up-glacier. We also acknowledge that our surface-lowering estimates incorporate any upward or downward flow of ice resulting from, for example, compressional flow over a zone of transition from active to inactive ice. We do not quantify emergence velocity as the ice thickness and surface velocity data required to do so (Immerzeel et al., 2014) are not available for an adequate number of glaciers in our sample.

3.6 Estimation of ELAs

We follow the approach of Braithwaite and Raper (2010) in using the median altitude of each glacier, information available in the RGI, to estimate the ELA of glaciers in our sample. Such an approach is most appropriate for glaciers in a state of balanced mass budget (Braithwaite and Raper, 2010; Braithwaite, 2015); thus the ELA estimates produced using this method could be considered an underestimate of modern-day ELAs given the negative state of mass balance of the majority of Himalayan glaciers. However, without measured mass balance records of adequate length against which to compare this or other (Braithwaite, 2015) ELA estimation methods, we take it as the best available approach. This is a method that has previously been employed in the Himalayas (Zhao et al., 2016), although we also note that this method cannot account for the input of avalanched material from steep valley walls – a substantial source of accumulation for Himalayan glaciers (Benn and Lehmkuhl, 2000). To estimate prospective future ELAs in response to temperature increases, we used vertical temperature gradients of $-8.5\,^{\circ}\mathrm{C\,km^{-1}}$ for the Pumqu catchment (Kattel et al., 2015) and $-5.4\,^{\circ}\mathrm{C\,km^{-1}}$ for the Dudh Koshi and Tama Koshi catchments (Immerzeel et al., 2014) to calculate prospective ELA shifts given different warming scenarios. We calculated ELAs for projected minimum, mean and maximum temperature increases under the four main RCP (Representative Concentration Pathways) scenarios outlined in the IPCC AR5 working group report (Collins et al., 2013).

4 Results

4.1 Glacier mass balance

The mean mass balance of all 32 glaciers in our sample was $-0.52 \pm 0.22\,\mathrm{m\,w.e.\,a^{-1}}$ between 2000 and 2015. There is considerable variability in the mass balance of glaciers with different terminus type (Figs. 3 and 4) and in the rates of

surface lowering through the altitudinal range of highlighted glaciers (Figs. 5 and 6). The mean mass balance of glaciers in catchments either side of the orographic divide are not markedly different, however.

Mean glacier mass balance (including land and lacustrine-terminating glaciers) was -0.51 ± 0.22 m w.e. a^{-1} in the Tama Koshi catchment, -0.58 ± 0.19 m w.e. a^{-1} in the Dudh Koshi catchment and -0.61 ± 0.24 m w.e. a^{-1} for glaciers flowing into the Pumqu catchment over the study period. The mean mass balance of nine lacustrine-terminating glaciers was -0.70 ± 0.26 m w.e. a^{-1}. This was 32 % more negative than land-terminating glaciers (mean mass balance of -0.53 ± 0.21 m w.e. a^{-1}) we include in our sample. The lowest mass loss rates occurred over debris-free glaciers at high altitude (5600–6200 m a.s.l) in the Pumqu catchment. The mean mass balance of these glaciers was -0.25 ± 0.22 m w.e. a^{-1} (Table S2) over the study period. Individual glacier mass balance estimates can be found in the Supplement.

4.2 Glacier surface lowering

The altitude at which maximum surface-lowering rates occurred differed depending only on glacier terminus type (Figs. 5 and 6). Across all three catchments, substantial surface lowering was pervasive over the middle portions of larger, land-terminating glaciers (Fig. 2). In the Dudh Koshi, surface-lowering rates are at their highest (-1.06 ± 0.10 m a^{-1}) around 5200 m a.s.l., although similar surface-lowering rates occurred between 5100 and 5300 m a.s.l (Fig. 5). In the Tama Koshi the highest rates of surface lowering (-1.08 ± 0.12 m a^{-1}) occurred at around 5400 m a.s.l (Fig. 5). In the Pumqu catchment, the highest mean surface-lowering rates again occurred between 5300 and 5400 m a.s.l.; the mean surface-lowering rate at this altitude was -1.62 ± 0.14 m a^{-1} over the study period. Surface-lowering rates over glaciers in the Pumqu catchment were higher than those in the Tama Koshi and Dudh Koshi catchments (Fig. 5) up to 5700 m a.s.l. (-1.24 ± 0.21 m a^{-1} at this altitude). Of note is the surface lowering over clean-ice areas high up on glaciers such as Ngozumpa, Rongbuk, Gyabrag and Bhote Kosi (Fig. 2). Surface lowering extended into tributary branches and the cirques of these largest glaciers. Individual glaciers showed much greater surface lowering, particularly in the Pumqu catchment. Gyabrag glacier lost an exceptional -3.33 ± 0.28 m a^{-1} between 5300 and 5400 m a.s.l (Fig. 5).

The maximum surface-lowering rates (-2.79 ± 0.29 m a^{-1}) occurred at the lowest elevations (between 4700 and 4900 m a.s.l) of lacustrine-terminating glaciers (Fig. 6). These nine glaciers all showed a linear surface-lowering gradient. We calculate the lowering gradient as surface elevation change per 100 m [m a^{-1} $(100\,\text{m})^{-1}$] vertical elevation change below the ELA. Lacustrine-terminating glaciers showed a lowering gradient of 0.30 m a^{-1} $(100\,\text{m})^{-1}$ over the study period. The lowering gradient of land-terminating glaciers was non-linear. Surface lowering was negligible around the terminus of most land terminating glaciers, with enhanced ice loss occurring further up-glacier where debris cover may have been thin or patchy. Lowering gradients for the area of land-terminating glaciers between the ELA and the altitude of maximum ice loss were 0.59, 0.66 and 0.38 m a^{-1} $(100\,\text{m})^{-1}$ for glaciers in the Pumqu, the Dudh Koshi and Tama Koshi catchments, respectively. Clean-ice glaciers also showed a linear lowering gradient – 0.77 m w.e. a^{-1} $(100\,\text{m})^{-1}$.

4.3 Glacier area changes and hypsometry

4.3.1 Total area changes

Two different patterns of ice area loss occurred over the study area during the last 15 years. Lacustrine-terminating glaciers and clean-ice glaciers all lost ice around their termini/calving fronts (Figs. 3 and 4) as glacial lakes expanded and termini receded. On average, lacustrine terminating glaciers each lost 0.54 ± 0.07 km^2 of ice (3.58 % of their total area) over the 15-year study period. Drogpa Nagtsang reduced in size by 2.37 km^2 (9.12 % of its total area; Table S3) as the associated rapidly forming lake expanded. Clean-ice glaciers lost 0.09 ± 0.03 km^2 of ice (1.31 % of their total area) on average.

Land-terminating glaciers lost little area as their surfaces lowered instead of their termini retreating. In the Tama Koshi and Dudh Koshi catchments, and in the Pumqu catchment, land-terminating glaciers lost a mean of 0.14 ± 0.12 km^2 (0.50 % of their total area), 0.09 ± 0.13 km^2 (0.60 % of their total area) and 0.41 ± 0.12 (1.77 % of their total area) of ice, respectively. Over these glaciers, any ice area loss was concentrated up-glacier, where their lateral margins dropped down inner moraine slopes and glacier tongues narrowed slightly.

Overall, our sample of glaciers lost 0.12 ± 0.04 % of their total area per year over the study period. This figure is identical to that of Bolch et al. (2008), who assessed area change over a smaller number of the same glaciers in our sample between 1962 and 2005. The annual area change rate we calculated is lower than those estimated by Thakuri et al. (2014) and references within. Thakuri et al. (2014) calculated a median annual surface area change rate of -0.42 ± 0.06 % a^{-1} in the Dudh Koshi catchment between 1962 and 2011. However, Thakuri et al. (2014) document area change over a number of smaller glaciers that are free of debris cover and therefore readily advance or retreat in response to climatic change; thus our estimates are not directly comparable.

4.3.2 Glacier hypsometry and approximate ELAs

The distribution of ice with elevation varies widely among the three studied catchments (Figs. 5 and 6). Debris-covered

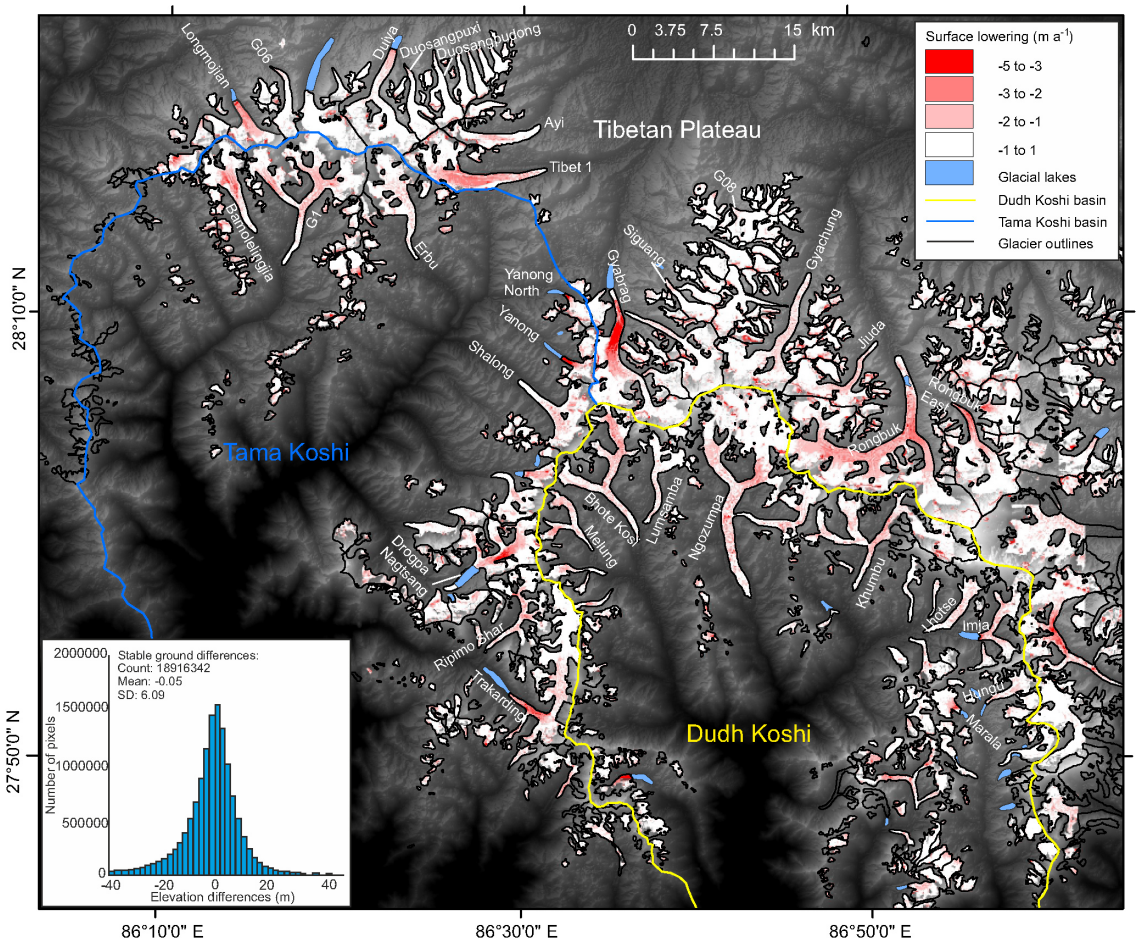

Figure 2. Glacier surface elevation change over the study area between 2000 and 2014/15. Also shown is a summary of off-glacier terrain differences. Areas of no data show the ASTER GDEM underlay.

glaciers of the Dudh Koshi catchment and the Pumqu catchment are typically very bottom heavy, with average HI scores of 2.63 and 2.34 (Table S1). Glacier hypsometry is concentrated between 4800 and 5500 m (Fig. 5) for the Dudh Koshi catchment and between 5600 and 6500 m in the Pumqu catchment. Notable exceptions are the Khumbu and Ngozumpa glaciers which store ice in broad accumulations zones above 7000 m (Tables S1 and S2). The majority of glaciers in the Tama Koshi have an equidimensional hypsometry (mean HI of 1.14), with most ice stored between 5300 and 5800 m. Glaciers in the Tama Koshi have broader accumulation basins than in the Dudh Koshi catchment, and the main glacier tongues are formed of multiple, smaller tributaries flowing from higher altitude in a number of cases (Fig. 1). The mean hypsometry (Fig. 6) of lacustrine-terminating glaciers shows no distinctive morphology as the sample is composed of glaciers from all three catchments in the study area. Clean-ice glaciers have a mean HI of 1.18 and could therefore be summarised as equidimensional, but the morphology of the five glaciers we assess is highly variable (see Table S3). In complete contrast to debris-covered glaciers, their ice is stored at higher mean altitudes on average, primarily between 6000 and 6500 m (Fig. 6).

We estimate the mean ELA of debris-covered glaciers in the Dudh Koshi and Tama Koshi catchments, and of our selection of glaciers in the Pumqu catchment to be 5477, 5568 and 6037 m a.s.l., respectively. We estimate the mean ELA of the five clean-ice glaciers in our sample to be 6216 m. Using those ELAs, the accumulation area ratio (AAR) (Dyurgerov et al., 2009) can be estimated for each glacier. We have calculated mean AARs of 0.41, 0.43 and 0.37 for debris-covered glaciers in the Dudh Koshi, Tama Koshi and Pumqu catchments. The mean AAR of clean-ice glaciers in our sample is 0.39.

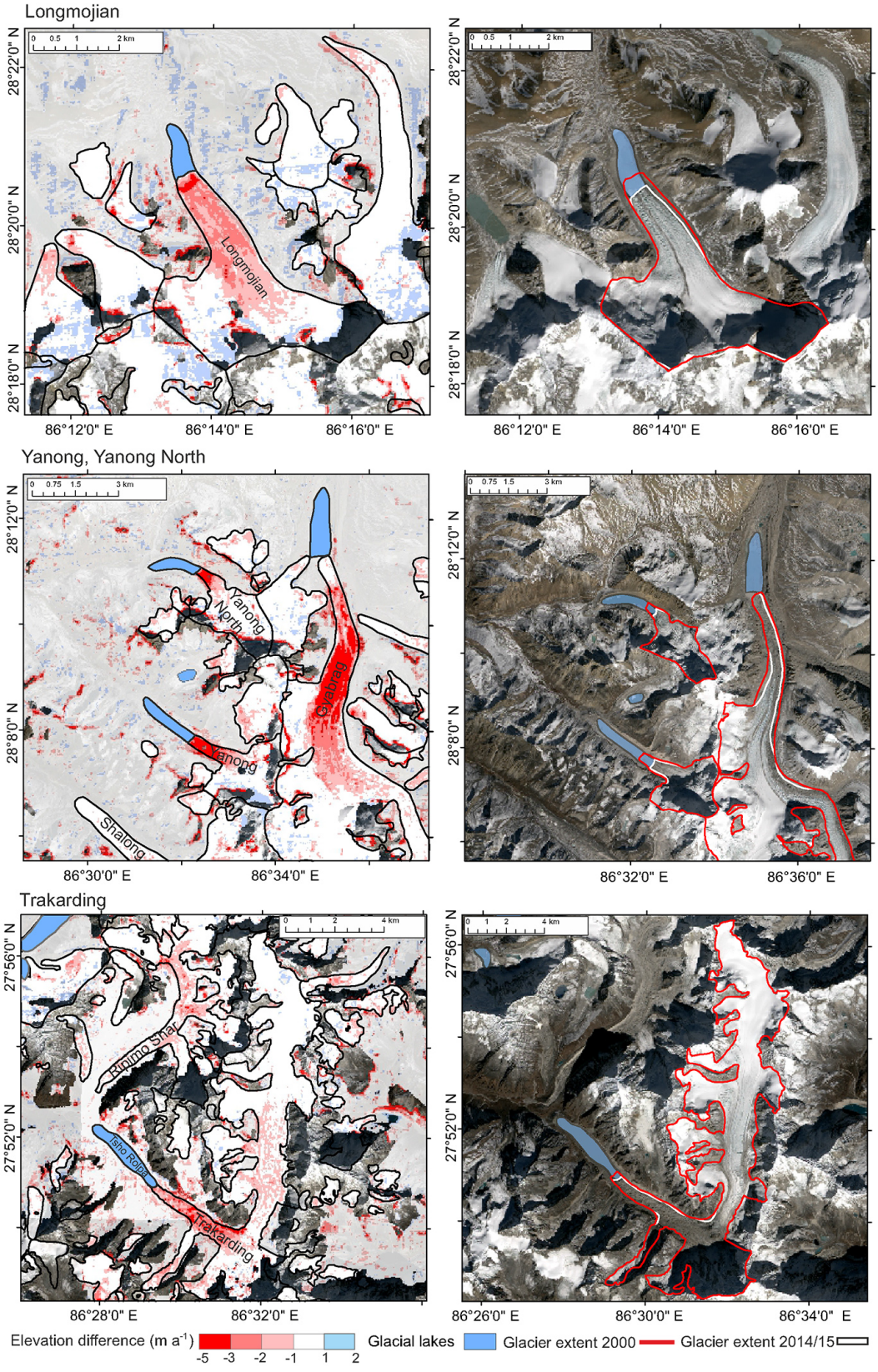

Figure 3. Examples of surface elevation change and total area change over the study period on lacustrine-terminating glaciers. Semi-transparent, off-glacier differences are also shown.

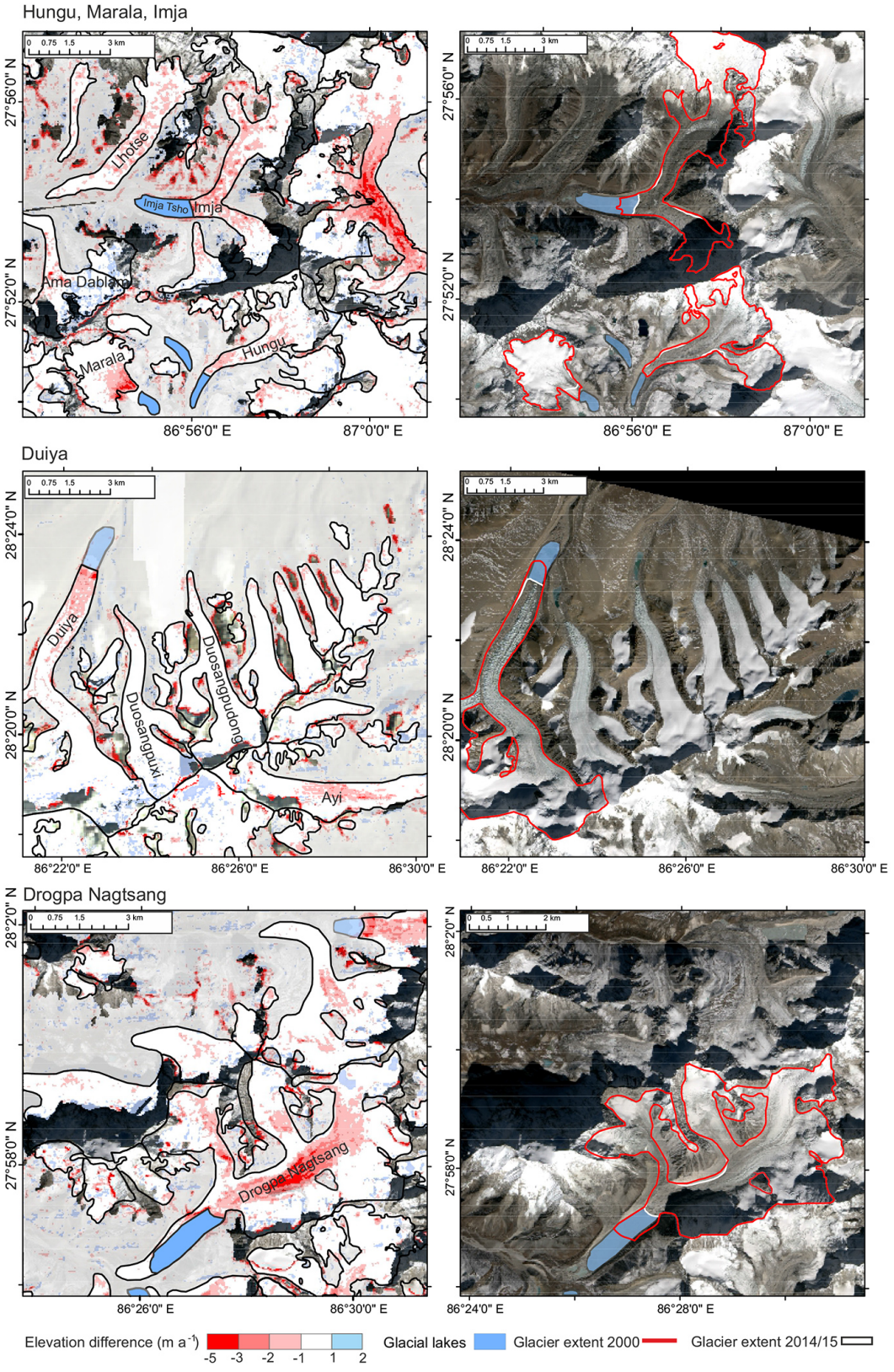

Figure 4. Further examples of glacier surface elevation change and total area change over the study period on lacustrine-terminating glaciers. Semi-transparent, off-glacier differences are also shown.

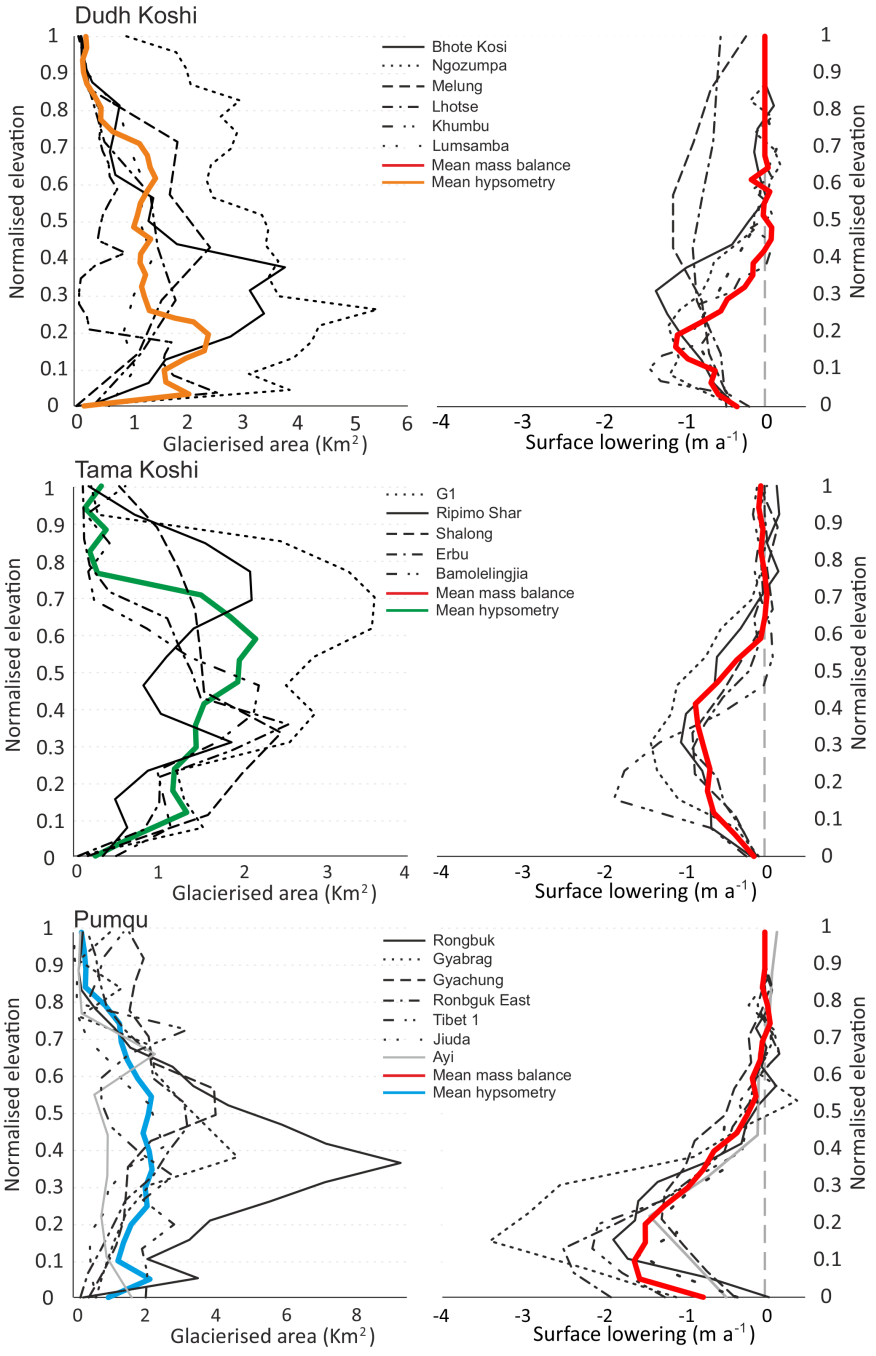

Figure 5. Surface elevation change and glacier hypsometry curves for all land terminating glaciers in the three different catchments of the study area.

5 Discussion

5.1 Variability in rates of ice loss across the orographic divide

The mean mass balance estimates we have derived for glaciers situated in catchments north and south of the main orographic divide are not markedly different. However, the contrast in maximum surface lowering (Fig. 5) from glaciers flowing north of the divide and the sustained surface lowering through a broader portion of their elevation range (Fig. 5) suggest that an additional or amplified process has driven glacier change north of the divide over recent decades. In this section we discuss possible topographic and climatic drivers

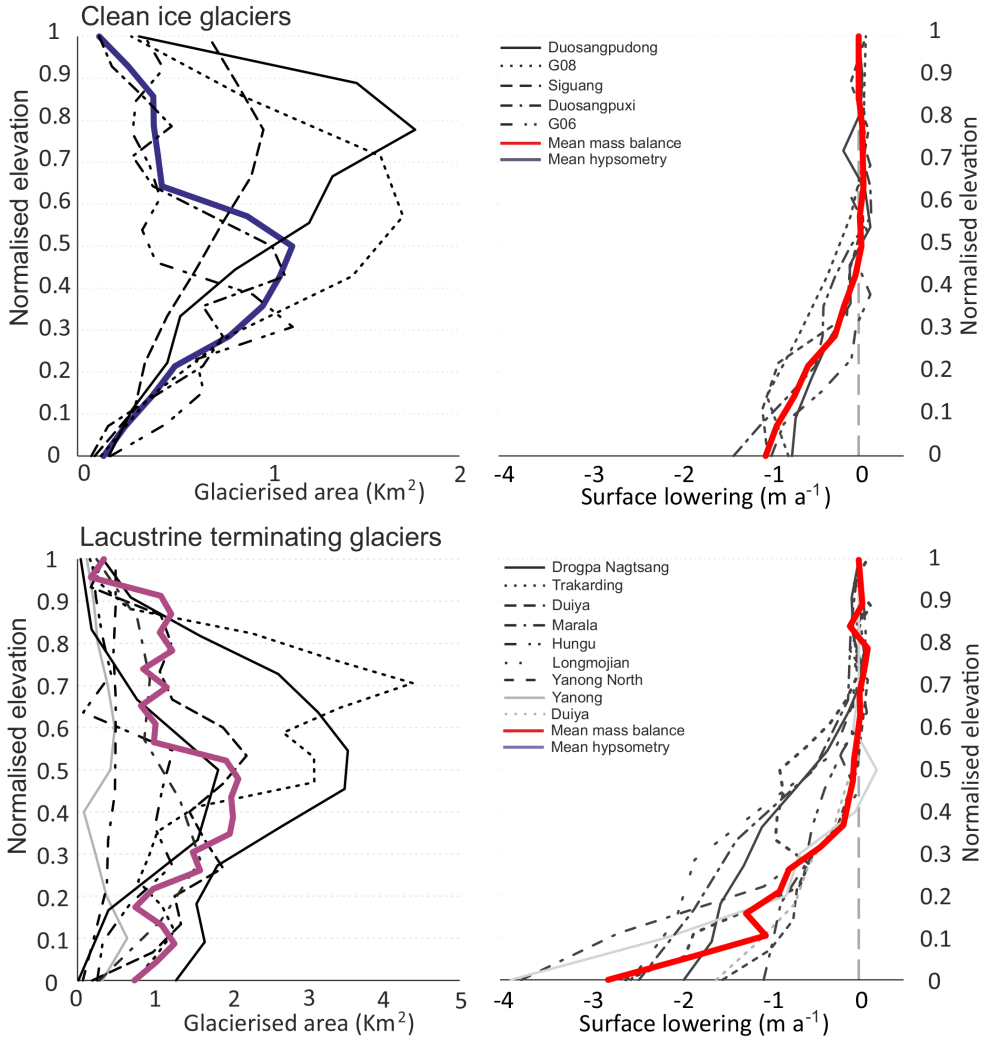

Figure 6. Surface-lowering and glacier hypsometry curves for clean ice and lacustrine-terminating glaciers in the study area.

of the difference in the rates of surface lowering across the range divide.

The Indian summer monsoon delivers a large proportion of total annual precipitation (up to 80 % of the total annual amount) to the Everest region of Nepal, resulting in high glacier sensitivity to temperature (Fujita, 2008; Sakai et al., 2015). The extreme topography in this region and the location of the orographic divide perpendicular to the prevailing monsoon result in rainfall peaks that are offset from the maximum elevations, with greatest rainfall occurring to the south of the divide and decreasing to the north across the Everest region (Bookhagen and Burbank, 2010; Wagnon et al., 2013). Around 449 mm a^{-1} of rainfall falls at the Pyramid research station (5000 m a.s.l.) at Khumbu Glacier (Salerno et al., 2015), whereas Dingri on the Tibetan Plateau (4300 m a.s.l.) to the north is much drier with 263 ± 84.3 mm a^{-1} of rainfall annually (Yang et al., 2011). Snowfall may follow a similar across-range gradient to rainfall, although falling snow may be carried further into the range by prevailing winds from the south. However, no reliable measurements of snowfall exist in this region with which to compare these trends. The north–south precipitation gradient across the orographic divide promotes differences in the response of these glaciers to climate change, such that those to the north are relatively starved of snow accumulation (Owen et al., 2009) and exposed to greater incoming radiative fluxes under generally clearer skies. Owen et al. (2009) suggest that this precipitation gradient resulted in greater glacier sensitivity to climate change on the northern slopes of the Himalayas during the Late Quaternary, with asymmetric patterns of ELA rise occurring since the Last Glacial Maximum (LGM).

During the period of this study (2000–2015), mean annual air temperatures have increased and rainfall amounts appear to have decreased in the Everest region (Salerno et al., 2015). At the Pyramid Observatory at Khumbu Glacier in the Dudh

Koshi catchment, increases in minimum ($+0.07\,^{\circ}\mathrm{C\,a^{-1}}$), maximum ($+0.009\,^{\circ}\mathrm{C\,a^{-1}}$) and mean ($+0.044\,^{\circ}\mathrm{C\,a^{-1}}$) annual air temperatures above 5000 m a.s.l. were observed between 1994 and 2013 (Salerno et al., 2015). At Dingri on the Tibetan Plateau, 60 km north-east of Mt Everest, increases in minimum ($+0.034\,^{\circ}\mathrm{C\,a^{-1}}$), maximum ($+0.041\,^{\circ}\mathrm{C\,a^{-1}}$) and mean ($+0.037\,^{\circ}\mathrm{C\,a^{-1}}$) annual air temperatures occurred over the same period (Salerno et al., 2015). Yang et al. (2011) also show a longer-term increase in the mean annual air temperature at Dingri, as do Shrestha et al. (1999) across the southern flank of the greater Himalayas. Between 1959 and 2007, the mean annual air temperature increased by $0.06\,^{\circ}\mathrm{C\,a^{-1}}$ at Dingri (Yang et al., 2011). Shestha et al. (1999) calculated an increase in the mean annual air temperature of $0.057\,^{\circ}\mathrm{C\,a^{-1}}$ between 1971 and 1994 across a number of sites in the greater Himalayas.

The snow-line altitude also appears to have increased recently on the southern flank of the Himalaya; Thakuri et al. (2014) showed a rapid ascent of the snow-line altitude in the Dudh Koshi between 1962 and 2011 (albeit through documenting transient snow lines from single scenes acquired at each epoch), and Khadka et al. (2014) suggest declining snow cover over the winter and spring months in the glacierised altitudinal ranges of the Tama Koshi catchment, between 2000 and 2009; a factor that may influence accumulation rates. Kaspari et al. (2008) showed decreasing accumulation recorded in an ice core collected from East Rongbuk Glacier Col (6518 m a.s.l.) on the northern side of Mt Everest between the 1970s and 2001.

We suggest that the north–south orographic precipitation gradient across the main divide may have caused greater surface-lowering rates on glaciers in the Pumqu catchment than those glaciers to the south over the study period. We also suggest that measured, contemporary increases in air temperature, observations of increasing snow-line altitude and declining accumulation are likely to enhance glacier mass loss across the range in future, but considerable unknown factors remain in the temporal evolution of debris cover extent and thickness (Thakuri et al., 2014), the strength of the summer monsoon in coming decades (e.g. Boos and Storelvmo, 2016), and the expansion or shrinkage of glacial lakes (see Sect. 5.3), all of which could additionally influence future glacier mass balance.

5.2 Comparison of mass balance estimates with other studies

Several other studies have generated geodetic mass balance estimates for glaciers of the Everest region over several different time periods. Bolch et al. (2011) generated balance estimates of -0.32 ± 0.08 and -0.79 ± 0.52 m w.e. $\mathrm{a^{-1}}$ for 10 glaciers to the south and west of Mt Everest over the periods 1970–2007 and 2002–2007, respectively. Nuimura et al. (2012) calculated a regional mass balance of -0.45 ± 0.25 m w.e. $\mathrm{a^{-1}}$ for 97 glaciers across the region over the period 1992–2008. Kääb et al. (2012) estimated a mass balance of -0.39 ± 0.11 m w.e. $\mathrm{a^{-1}}$ for a $3^{\circ} \times 3^{\circ}$ cell centred on the Everest region between 2003 and 2008. Gardelle et al. (2013) calculated a slightly less negative mass balance of -0.26 ± 0.13 m w.e. $\mathrm{a^{-1}}$ between 1999 and 2011, although the SRTM penetration correction applied by Gardelle et al. (2013) may have caused a bias towards a less negative mass balance (Kääb et al., 2012; Barundun et al., 2015). The regional mass balance of -0.52 ± 0.22 m w.e. $\mathrm{a^{-1}}$ that we have calculated suggests that the mass loss rates measured by Nuimura et al. (2012) and Kääb et al. (2012) have been sustained and possibly increased in recent years (Table 3), as Bolch et al. (2011) also suggest.

On the Tibetan Plateau, Neckel et al. (2014) estimated the mass balance of glaciers on the northern side of the orographic divide in the central and eastern Himalayas (their subregion G) to be -0.66 ± 0.36 m w.e. $\mathrm{a^{-1}}$ between 2003 and 2009. The mass balance of glaciers in our sample within the same region was -0.59 ± 0.27 m w.e. $\mathrm{a^{-1}}$ between 2000 and 2015. Ye et al. (2015) estimated glacier mass balance to be -0.40 ± 0.27 m w.e. $\mathrm{a^{-1}}$ in the Rongbuk catchment between 1974 and 2006, suggesting that glacier ice mass loss rates may have increased over the last decade in this area of the Tibetan Plateau (Table 3).

Table 3. Mass balance estimates (from geodetic and altimetric studies) for the broader Everest region and comparable subregions/ catchments.

Time period and area	Mass balance estimate (m w.e. $\mathrm{a^{-1}}$)	Study
Dudh Koshi		
1970–2007	-0.32 ± 0.08	Bolch et al. (2011)
1992–2008	-0.45 ± 0.25	Nuimura et al. (2012)
2002–2007	-0.79 ± 0.52	Bolch et al. (2011)
2000–2015	-0.58 ± 0.19	This study
Pumqu (Tibetan Plateau)		
1974–2006	-0.40 ± 0.27	Ye et al. (2015)
2003–2009	-0.66 ± 0.32	Neckel et al. (2014)
2000–2015	-0.61 ± 0.24	This study
Tama Koshi		
2000–2015	-0.51 ± 0.22	This study
Everest region		
1999–2011	-0.26 ± 0.13	Gardelle et al. (2013)
2003–2008	-0.39 ± 0.11	Kääb et al. (2012)
2000–2015	-0.52 ± 0.22	This study

5.3 The influence of glacial lakes on glacier mass balance

Only Nuimura et al. (2012) have directly compared mass loss rates of lacustrine and land-terminating glaciers in the study area, showing faster surface-lowering rates over Imja and Lumding glaciers in the Dudh Koshi catchment. Our data confirm that lacustrine-terminating glaciers can indeed lose ice at a much faster rate than land-terminating glaciers. The variability in the mass balance of the nine lacustrine-terminating glaciers (Fig. 6) we highlight suggests the fastest mass loss rates occur in the later stages of lake development. Glaciers such as the Yanong and Yanong North, in the Tama Koshi catchment, sit behind large proglacial lakes and are in a state of heavily negative mass balance (-0.76 ± 0.18 and -0.62 ± 0.25 m w.e. a^{-1}, respectively). Their surfaces lowered by 3 m a^{-1} or more over their lower reaches (Fig. 6) over the study period. These glaciers are now relatively small and steep and no longer possess a debris-covered tongue, and so may represent the end product of debris-covered glacier wastage described by Benn et al. (2012). In contrast, glaciers such as Duiya, in the Pumqu catchment, currently has only a small lake at its termini, showed moderate area losses (0.5 km^2 or 4.28 % of its total area) and moderately negative mass balance (-0.45 ± 0.13 m w.e. a^{-1}) over the study period. Continued thinning of the terminal regions of glaciers with smaller glacial lakes would lead to a reduction in effective pressure, an increase in longitudinal strain and therefore flow acceleration (Benn et al., 2007). The retreat of the calving front up-valley into deeper bed topography may also increase calving rates (Benn et al., 2007), and a combination of both of these processes would lead to enhanced ice loss. Very few surface velocity data exist for lacustrine-terminating debris-covered glaciers. Only Quincey et al. (2009) measured high surface velocities (25 m a^{-1} or more) over Yanong glacier (their Fig. 4d), suggesting it is possible for lacustrine-terminating glaciers to become more dynamic in the later stages of lake development in the Himalayas. Conversely, Thakuri et al. (2016) have shown flow deceleration of glaciers that coalesce to terminate in Imja Tsho over the period 1992–2014 and suggest that reduced accumulation caused by decreasing precipitation is responsible for diminishing surface flow on this glacier. Clearly, more expansive investigation into the evolving dynamics of lacustrine-terminating glaciers in the Himalayas is required if we are to better understand their potential future mass loss.

5.4 Glacier stagnation

A number of studies (Luckman et al., 2007; Scherler et al., 2008, 2011; Quincey et al., 2009) have shown how many glaciers in the Everest region appear to be predominantly stagnant, with large parts of the long, debris-covered glacier tongues in the area showing little to no flow. Watson et al. (2016) have documented an increasing number and total area of supraglacial melt ponds over a number of the same glaciers studied by Quincey et al. (2009) in the Dudh Koshi catchment (Khumbu, Ngozumpa, Lhotse, Imja and Ama Dablam), since the early 2000s. Over these glaciers, our data show a very distinctive surface-lowering pattern (Fig. 2), with localised, heterogenous surface lowering appearing to mirror the distribution of large supraglacial ponds and ponds networks. This ice loss pattern is prevalent on the Erbu, Gyachung, Jiuda, Shalong and G1 glaciers (Fig. 2), and high-resolution imagery available on Google Earth shows that these glaciers also have well-developed networks of supraglacial ponds. We would therefore suggest that large parts of the biggest glaciers in the Tama Koshi catchment and in the Pumqu catchment are also stagnant and may see increasing supraglacial meltwater storage in the future, similar to that documented by Watson et al. (2016).

5.5 Susceptibility of glaciers to future mass loss

ELA ascent in response to temperature increases

The coincidence of maximum surface-lowering rates with the altitude of maximum hypsometry in the Dudh Koshi catchment (Fig. 5) suggests large glacier mass losses in this catchment. Sustained and prolonged mass loss may lead to a bimodal hypsometry here, with the physical detachment of debris-covered glacier tongues and their high-elevation accumulation zones a possibility (Rowan et al., 2015; Shea et al., 2015). Surface-lowering maxima in the Tama Koshi catchment presently occur at a slightly lower elevation range than the main hypsometric concentration, and across lower reaches of glacier tongues in the Pumqu catchment.

Figure 7 shows projected AARs, averaged across each catchment, in response to different levels of temperature rise. These predictions are based on published lapse rates (Immerzeel et al., 2014; Kattel et al., 2015) that may be spatially variable and assume no changes in precipitation type or amount or any variability in the contribution of avalanches to accumulation.

To allow a comparison of our results with similar estimates of other studies (Shea et al., 2015; Rowan et al., 2015), we focus specifically on ELA rise resulting from RCP 4.5 minimum and maximum projected warming of annual air temperatures (+0.9 to +2.3 °C by 2100). Such temperature increases would cause a rise in ELA of between 165 and 425 m in the Dudh and Tama Koshi catchments and between 107 and 270 m of ELA ascent over glaciers in the Pumqu catchment. A rise in ELAs would most significantly affect the Tama Koshi catchment glaciers, which currently have the highest catchment-averaged AAR, 0.43. RCP 4.5 warming could cause AAR decrease to 0.29 and 0.08, respectively, in the Tama Koshi catchment. The greater altitudinal range and higher accumulation zones of glaciers in the Dudh Koshi catchment and in the Pumqu catchment would dampen the

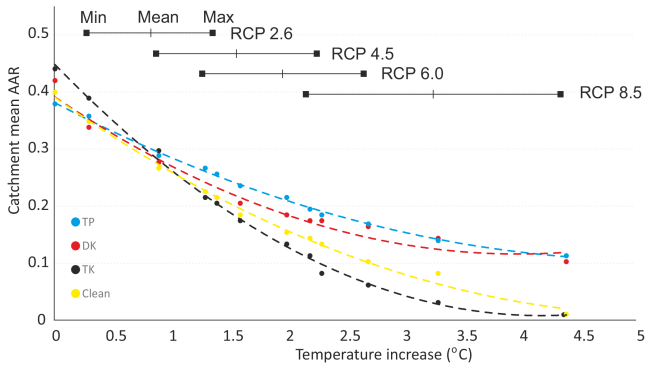

Figure 7. Projected AARs (averaged across each catchment) based on different scenarios of temperature increase relative to the present day and accompanying ELA rise. Temperature rise scenarios have been used from the IPCC AR5 Working Group report. P is Pumqu, DK is Dudh Koshi, TK is Tama Koshi and Clean is clean-ice glaciers. Each point represents a projected AAR given minimum, mean or maximum temperature rise under each RCP scenario.

effects of a rise in ELA on glacier mass balance, with AAR adjustment occurring more gradually (Fig. 7). AARs could decrease to 0.27 or 0.17 in the Dudh Koshi and to 0.29 or 0.18 in the Pumqu catchment. ELA rise in response to this particular warming scenario would mean a 12–30 % increase in the total glacierised area below the ELA in the Pumqu catchment, a 24–61 % increase in the Tama Koshi catchment and a 23–40 % increase in the Dudh Koshi catchment. Should more substantial temperature increases occur (> 2 °C warming), AARs could reduce to zero on a number of individual glaciers, and the ELA could rise to near-maximum glacier altitudes in the Tama Koshi catchment. Clean-ice glacier AAR adjustment may be rapid given their limited altitudinal range (Fig. 7).

Glacier AAR is a parameter strongly related to long-term mass balance for typical alpine glaciers (König et al., 2014), although the effect of a diminishing AAR may be dampened on Himalayan glaciers given the large input of avalanche material derived from high surrounding headwalls (Iturrizaga, 2011). Since data on the rates of avalanching in high-mountain environments such as the Himalayas are sparse (Benn and Lehmkuhl, 2000), the impact of predicted AAR reduction remains somewhat uncertain.

6 Conclusions

DEM differencing has revealed substantial mass loss from many large, debris-covered glaciers in the central Himalayas over the last 15 years. Geodetic mass balance estimates have been calculated for 32 glaciers across three different catchments around the Everest region. We found similarly negative mass budgets for glaciers flowing onto the southern flank of the Himalayas, in the Tama Koshi (-0.51 ± 0.22 m w.e. a^{-1}) and Dudh Koshi (-0.58 ± 0.19 m w.e. a^{-1}) catchments, and in the Pumqu catchment (-0.61 ± 0.24 m w.e. a^{-1}).

The division of our sample of glaciers depending on their terminus type shows contrasting mass loss rates between land and lacustrine-terminating glaciers. The mean mass balance of nine lacustrine-terminating glaciers we assessed was -0.70 ± 0.26 m w.e. a^{-1}, 32 % more negative than land-terminating glaciers (mean mass balance of -0.53 ± 0.21 m w.e. a^{-1}). The mass balance of nine lacustrine-terminating glaciers ranged from -0.91 ± 0.22 to -0.45 ± 0.13 m w.e. a^{-1} and we would suggest that glacial lakes in the region are at different stages of expansion. Accelerating mass loss is likely from several of these lacustrine-terminating glaciers, the termini of which will retreat into deeper lake water.

Surface-lowering curves show that the maximum-lowering rate (-1.62 ± 0.14 m a^{-1} between 5300 and 5400 m.a.s.l.) of glaciers in the Pumqu catchment was well above the maximum-lowering rate of glaciers flowing south of the orographic divide (-1.06 ± 0.10 m a^{-1} between 5200 and 5300 m a.s.l. in the Dudh Koshi catchment, -1.08 ± 0.12 m a^{-1} between 5200 and 5300 m a.s.l. in the Tama Koshi catchment), and that glaciers in the Pumqu catchment are losing ice over a much broader altitudinal range than their south-flowing counterparts. We suggest that the across-range contrast in annual precipitation amount, combined with rising mean air temperatures over recent decades may have caused greater ice loss rates from the north-flowing glaciers.

Predicted warming in the Everest region will lead to increased ELAs and, depending on glacier hypsometry, substantial increases in the size of ablation areas. We show that glaciers of the Tama Koshi catchment will see the greatest reduction in glacier AAR due to their equidimensional hypsometry and more limited elevation range in comparison to glaciers of the Dudh Koshi or in the Pumqu catchment. A warming of +0.9 to +2.3 °C by 2100 (IPCC RCP 4.5) would decrease glacier AAR to 0.29 or 0.08 in the Tama Koshi catchment, 0.27 or 0.17 in the Dudh Koshi catchment and 0.29 or 0.18 in the Pumqu catchment.

Our findings are important for two reasons. First, they suggest that glacial lake growth and current glacial lake expansion that have been documented across the Himalayas could be accompanied by amplified glacier mass loss in the near future. Second, they show that glacier AAR adjustment in response to predicted warming across the Himalayas could be spatially very variable, complicating the prediction of future glacier meltwater run-off contribution from river catchments across the region.

7 Data availability

DEM difference data are available upon request. Please contact Owen King for this purpose (gy08ok@leeds.ac.uk). SETSM DEMs are available for download from http://www.pgc.umn.edu/elevation. The SRTM dataset is available from https://lta.cr.usgs.gov/SRTM1Arc via https://earthexplorer.usgs.gov/ (USGS, 2016). EGM2008 gridded data are available from http://earth-info.nga.mil/GandG/wgs84/gravitymod/egm2008/egm08_gis.html.

The Supplement related to this article is available online at doi:10.5194/tc-11-407-2017-supplement.

Author contributions. Owen King, Duncan J. Quincey and Jonathan L. Carrivick designed the study. Owen King carried out all data processing and analysis. Owen King, Duncan J. Quincey, Jonathan L. Carrivick and Ann V. Rowan wrote the paper.

Competing interests. The authors declare that they have no conflict of interest.

Acknowledgements. Owen King is a recipient of a NERC DTP PhD studentship. We are grateful to Benjamin Robson for his comments on an early version of the paper, and for guidance on the use of SETSM data from Ian Howat. We finally thank Tobias Bolch, Joseph Shea and an anonymous reviewer for their thorough and constructive assessments of the manuscript.

Edited by: T. Bolch
Reviewed by: J. M. Shea and one anonymous referee

References

Arendt, A., Echelmeyer, K., Harrison, W., Lingle, C., Zirnheld, S., Valentine, V., Ritchie, B., and Druckenmiller, M.: Updated estimates of glacier volume changes in the western Chugach Mountains, Alaska, and a comparison of regional extrapolation methods, J. Geophys. Res.-Earth, 111, F03019, doi:10.1029/2005JF000436, 2006.

Arendt, A., Bliss, A., Bolch, T., Cogley, J. G., Gardner, A. S., Hagen, J.-O., Hock, R., Huss, M., Kaser, G., Kienholz, C., Pfeffer, W. T., Moholdt, G., Paul, F., Radić, V., Andreassen, L., Bajracharya, S., Barrand, N.E., Beedle, M., Berthier, E., Bhambri, R., Brown, I., Burgess, E., Burgess, D., Cawkwell, F., Chinn, T., Copland, L., Davies, B., De Angelis, H., Dolgova, E., Earl, L., Filbert, K., Forester, R., Fountain, A. G., Frey, H., Giffen, B., Glasser, N. F., Guo, W. Q., Gurney, S., Hagg, W., Hall, D., Haritashya, U. K., Hartmann, G., Helm, C., Herreid, S., Howat, I., Kapustin, G., Khromova, T., König, M., Kohler, J., Kriegel, D., Kutuzov, S., Lavrentiev, I., LeBris, R., Liu, S. Y., Lund, J., Manley, W., Marti, R., Mayer, C., Miles, E. S., Li, X., Menounos, B., Mercer, A., Mölg, N., Mool, P., Nosenko, G., Negrete, A., Nuimura, T., Nuth, C., Pettersson, R., Racoviteanu, A., Ranzi, R., Rastner, P., Rau, F., Raup, B., Rich, J., Rott, H., Sakai, A., Schneider, C., Seliverstov, Y., Sharp, M., Sigurðsson, O., Stokes, C., Way, R. G., Wheate, R., Winsvold, S., Wolken, G., Wyatt, F., and Zheltyhina, N.: Randolph Glacier Inventory – A Dataset of Global Glacier Outlines: Version 5.0. Global Land Ice Measurements from Space, Digital Media, Boulder Colorado, USA, 2015.

Asahi, K.: Inventory and recent variations of glaciers in the eastern Nepal Himalayas, J. Jpn. Soc. Snow Ice, 63, 159–169, 2001.

Bajracharya, S. R. and Mool, P.: Glaciers, glacial lakes and glacial lake outburst floods in the Mount Everest region, Nepal, Ann. Glaciol., 50, 81–86, 2009.

Bajracharya, S. R., Maharjan, S. B., Shrestha, F., Guo, W., Liu, S., Immerzeel, W., and Shrestha, B.: The glaciers of the Hindu Kush Himalayas: current status and observed changes from the 1980s to 2010, Int. J. Water Resour. D., 31, 161–173, 2015.

Barundun, M., Huss, M., Sold, L., Farinotti, D., Azisov, E., Salzmann, N., Usubaliev, R., Merkushkin, A., and Hoelzle, M.: Reanalysis of seasonal mass balance at Abramov glacier 1968–2014, J. Glaciol., 61, 1103–1117, doi:10.3189/2015JoG14J239, 2015.

Basnet, S., Kulkarni, A., and Bolch, T.: The influence of debris cover and glacial lakes on the recession of glaciers in the Sikkim Himalaya, India, J. Glaciol., 59, 1035–1046, 2013.

Benn, D. I. and Lehmkuhl, F.: Mass balance and equilibrium line altitudes of glaciers in high mountain environments, Quatern. Int., 65/66, 15–29, 2000.

Benn, D. I., Warren, C. R., and Mottram, R. H.: Calving processes and the dynamics of calving glaciers, Earth-Sci. Rev., 82, 143–179, 2007.

Benn, D. I., Bolch, T., Hands, K., Gulley, J., Luckman, A., Nicholson, L. I., Quincey, D., Thompson, S., Toumi, R., and Wiseman, S.: Response of debris-covered glaciers in the Mount Everest region to recent warming, and implications for outburst flood hazards, Earth-Sci. Rev., 114, 156–174, 2012.

Berthier, E., Arnaud, Y., Vincent, C., and Remy, F.: Biases of SRTM in high-mountain areas: Implications for the monitoring of glacier volume changes, Geophys. Res. Lett., 33, L08502, doi:10.1029/2006GL025862, 2006.

Berthier, E., Arnaud, Y., Kumar, R., Ahmad, S., Wagnon, P., and Chevallier, P.: Remote sensing estimates of glacier mass balances in the Himachal Pradesh (Western Himalaya, India), Remote Sens. Environ., 108, 327–338, 2007.

Berthier, E., Cabot, V., Vincent, C., and Six, D.: Decedal region-wide and glacier wide mass balances derived from multi-temporal ASTER satellite digital elevation models. Validation over the Mont-Blanc area, Front. Earth Sci., 4, 63, doi:10.3389/feart.2016.00063, 2016.

Bhutiyana, M. R. Kale, V. S., and Pawar, N. J.: Climate change and the precipitation variations in the northwestern Himalaya: 1866–2006, Int. J. Climatol., 30, 535–548, 2010.

Bolch, T., Buchroithner, M., Pieczonka, T., and Kunert, A.: Planimetric and volumetric glacier changes in the Khumbu Himal, Nepal, since 1962 using Corona, Landsat TM and ASTER data,

J. Glaciol., 54, 592–600, doi:10.3189/002214308786570782, 2008.

Bolch, T., Pieczonka, T., and Benn, D. I.: Multi-decadal mass loss of glaciers in the Everest area (Nepal Himalaya) derived from stereo imagery, The Cryosphere, 5, 349–358, doi:10.5194/tc-5-349-2011, 2011.

Bolch, T., Kulkarni, A., Kääb, A., Huggel, C., Paul, F., Cogley, J. G., Frey, H., Kargel, J. S., Fujita, K., Scheel, M., Bajracharya, S., and Stoffel, M.: The State and Fate of Himalayan Glaciers, Science, 336, 310–314, 2012.

Bollasina, M. A., Ming, Y., and Ramaswamy, V.: Anthropogenic Aerosols and the Weakening of the South Asian Summer Monsoon, Science, 334, 502–505, 2011.

Bookhagen, B. and Burbank, D.: Toward a complete Himalayan hydrologica budget: Spatiotemporal distribution of snowmelt and rainfall and thir impact on river discharge, J. Geophys. Res., 115, F03019, doi:10.1029/2009JF001426, 2010.

Boos, W. R. and Storelvmo, T.: Near-linear response of mean monsoon strength to a broad range of radiative forcings, P. Natl. Acad. Sci. USA, 113, 1510–1515, 2016.

Braithwaite, R. J.: From Doktor Kurowski's Schneegrenze to our modern glacier equilibrium line altitude (ELA), The Cryosphere, 9, 2135–2148, doi:10.5194/tc-9-2135-2015, 2015.

Braithwaite, R. J. and Raper, S. C. B.: Estimating equilibrium-line altitude (ELA) from glacier inventory data, Ann. Glaciol., 50, 127–132, 2010.

Buchroithner, M. F., Jentsch, G., and Wanivenhaus, B.: Monitoring of recent geological events in the Khumbu area (Himalaya, Nepal) by digital processing of landsat MSS data, Rock Mech., 15, 181–197, 1982.

Carrivick, J. L. and Tweed, F. S.: Proglacial lakes: character, behaviour and geological importance, Quaternary Sci. Rev., 78, 34–52, 2013.

Che, T., Xaio, L., and Liou, Y.-A.: Changes in Glaciers and Glacial Lakes and the Identification of Dangerous Glacial Lakes in the Pumqu River Basin, Xizang (Tibet), Adv. Meteorol., 2014, 903709, doi:10.1155/2014/903709, 2014.

Collins, M., Knutti, R., Arblaster, J., Dufresne, J.-L., Fichefet, T., Friedlingstein, P., Gao, X., Gutowski, W. J., Johns, T., Krinner, G., Shongwe, M., Tebaldi, C., Weaver, A. J., and Wehner, M.: Long-term Climate Change: Projections, Commitments and Irreversibility, in: Climate Change 2013: The Physical Science Basis. Contribution of Working Group I to the Fifth Assessment Report of the Intergovernmental Panel on Climate Change, edited by: Stocker, T. F., Qin, D., Plattner, G.-K., Tignor, M., Allen, S. K., Boschung, J., Nauels, A., Xia, Y., Bex, V., and Midgley, P. M., Cambridge University Press, Cambridge, UK and New York, NY, USA, 2013.

Dyurgerov, M., Meier, M. F., and Bahr, D. B.: A new index of glacier area change: a tool for glacier monitoring, J. Glaciol., 55, 710–716, 2009.

Farr, T. G., Rosen, P. A., Carop, E., Crippen, R., Duren, R., Hensley, S., Korbick, M., Paller, M., Rodriguez, E., Roth, L., Seal, D., Shaffer, S., Shimada, J., Umland, J., Werner, M., Oskin, M., Burbank, D., and Alsdorf, D.: The Shuttle Radar Topography Mission, Rev. Geophys., 45, RG2004, doi:10.1029/2005RG000183, 2007.

Frey, H., Machguth, H., Huss, M., Huggel, C., Bajracharya, S., Bolch, T., Kulkarni, A., Linsbauer, A., Salzmann, N., and Stoffel, M.: Estimating the volume of glaciers in the Himalayan–Karakoram region using different methods, The Cryosphere, 8, 2313–2333, doi:10.5194/tc-8-2313-2014, 2014.

Fujita, K.: Effect of precipitation seasonality on climatic sensitivity of glacier mass balance, Earth Planet. Sc. Lett., 276, 14–19, doi:10.1016/j.epsl.2008.08.028, 2008.

Furbish, D. J. and Andrews, J. T.: The use of hypsometry to indicate long term stability and response of valley glaciers to changes in mass transfer, J. Glaciol., 30, 199–211, 1984.

Gardelle, J., Arnaud, Y., and Berthier, E.: Contrasted evolution of glacial lakes along the Hindu Kush Himalaya mountain range between 1990 and 2009, Global Planet. Change, 75, 47–55, 2011.

Gardelle, J., Berthier, E., and Arnaud, Y.: Slight mass gain of Karakorum glaciers in the early 21st century, Nat. Geosci., 5, 322–325, doi:10.1038/ngeo1450, 2012.

Gardelle, J., Berthier, E., Arnaud, Y., and Kääb, A.: Region-wide glacier mass balances over the Pamir-Karakoram-Himalaya during 1999–2011, The Cryosphere, 7, 1263–1286, doi:10.5194/tc-7-1263-2013, 2013.

Hambrey, M. J., Quincey, D. J., Glasser, N. F., Reynolds, J. M., Richardson, S. J., and Clemmens, S.: Sedimentological, geomorphological and dynamic context of debris-mantled glaciers, Mount Everest (Sagarmatha) region, Nepal, Quaternary Sci. Rev., 27, 2361–2389, 2008.

Huss, M.: Density assumptions for converting geodetic glacier volume change to mass change, The Cryosphere, 7, 877–887, doi:10.5194/tc-7-877-2013, 2013.

Huss, M. and Hock, R.: A new model for global glacier change and sea-level rise, Front. Earth Sci., 3, 54, doi:10.3389/feart.2015.00054, 2015.

Immerzeel, W. W., Van Beek, L. P. H., and Bierkens, M. F. P.: Climate Change Will Affect the Asian Water Towers, Science, 328, 1382–1385, 2010.

Immerzeel, W. W., Kraaijenbrink, M., Shea, J. M., Shrestha, A. B., Pellicciotti, F., Bierkens, M. F. P., and de Jong, S. M.: High-resolution monitoring of Himalayan glacier dynamics using unmanned aerial vehicles, Remote Sens. Environ., 150, 93–103, 2014.

Iturrizaga, L.: Trends in 20th century and recent glacier fluctuations in the Karakoram Mountains, Z. Geomorphol., 55, 203–231, 2011.

Jin, R., Li, X., Che, T., Wu, L., and Mool, P.: Glacier area changes in the Pumqu river basin, Tibetan Plateau, between the 1970s and 2001, J. Glaciol., 51, 607–610, 2005.

Jiskoot, H., Curran, C. J., Tessler, D. L., and Shenton, L. R.: Changes in Clemenceau Icefield and Chaba Group glaciers, Canada, related to hypsometry, tributary detachment, length, slope and area & aspect relations, Ann. Glaciol., 50, 133–143, 2009.

Kääb, A., Berthier, E., Nuth, C., Gardelle, J., and Arnaud, Y.: Contrasting patterns of early twenty-first-century glacier mass change in the Himalayas, Nature, 488, 495–498, 2012.

Kääb, A., Treichler, D., Nuth, C., and Berthier, E.: Brief Communication: Contending estimates of 2003–2008 glacier mass balance over the Pamir–Karakoram–Himalaya, The Cryosphere, 9, 557–564, doi:10.5194/tc-9-557-2015, 2015.

Kaspari, S., Hooke, R. LeB., Mayewski, P. A., Kang, S. C., Hou, S. G., and Qin, D. H.: Snow accumulation rate on Qomolangma (Mount Everest), Himalaya: synchroneity with sites across the

Tibetan Plateau on 50–100 year timescales, J. Glaciol., 54, 343–352, doi:10.3189/002214308784886126, 2008.

Kattel, D. B., Yao, T., Yang, W., Gao, Y., and Tian, L.: Comparison of temperature lapse rates from the northern to the southern slopes of the Himalayas, Int. J. Climatol., 35, 4431–4443, 2015.

Khadka, D., Babel, M. S., Shrestha, S., and Tripathi, N. K.: Climate change impact on glacier and snow melt and runoff in Tamakoshi basin in the Hindu Kush Himalayan (HKH) region, J. Hydrol., 511, 49–60, 2014.

König, M., Nuth, C., Kohler, J., Moholdt, G., and Pettersen, R.: A digital glacier database for svalbard, in: Global Land Ice Measurements from Space, edited by: Kargel, S. J., Leonard, J. G., Bishop, P. M., Kääb, A., and Raup, H. B., Springer Berlin Heidelberg, Germany, 2014.

Larsen, C. F., Motyka, R. J., Arendt, A. A., Echelmeyer, K. A., and Geissler, P. E.: Glacier changes in southeast Alaska and northwest British Columbia and contribution to sea level rise, J. Geophys. Res.-Earth, 112, F01007, doi:doi:10.1029/2006JF000586, 2007.

Luckman, A., Quincey, D., and Bevan, S.: The potential of satellite radar interferometry and feature tracking for monitoring flow rates of Himalayan glaciers, Remote Sens. Environ., 111, 172–181, 2007.

Lutz, A. F., Immerzeel, W. W., Gobiet, A., Pellicciotti, F., and Bierkens, M. F. P.: Comparison of climate change signals in CMIP3 and CMIP5 multi-model ensembles and implications for Central Asian glaciers, Hydrol. Earth Syst. Sci., 17, 3661–3677, doi:10.5194/hess-17-3661-2013, 2013.

Neckel, N., Kropacek, J., Bolch, T., and Hochschild, V.: Glacier-mass changes on the Tibetan Plateau 2003–2009 derived from ICESat laser altimetry measurements, Environ. Res. Lett., 9, 014009, doi:10.1088/1748-9326/9/1/014009, 2014.

Noh, M. J. and Howat, I. M.: Automated stereo-photogrammetric DEM generation at high latitudes: Surface Extraction with TIN-based Search-space Minimization (SETSM) validation and demonstration over glaciated regions, GISci. Remote Sens., 52, 198–217, 2015.

Nuimura, T., Fujita, K., Yamaguchi, S., and Sharma, R. R.: Elevation changes of glaciers revealed by multitemporal digital elevation models calibrated by GPS survey in the Khumbu region, Nepal Himalaya, 1992–2008, J. Glaciol., 58, 648–656, 2012.

Nuth, C. and Kääb, A.: Co-registration and bias corrections of satellite elevation data sets for quantifying glacier thickness change, The Cryosphere, 5, 271–290, doi:10.5194/tc-5-271-2011, 2011.

Owen, L. A. Robinson, R., Benn, D. I., Finkel, R. C., Davis, N. K., Yi, C., Putkonen, J., Li, D., and Murray, A. S.: Quaternary glaciation of Mount Everest, Quaternary Sci. Rev., 28, 1412–1433, 2009.

Peduzzi, P., Herold, C., and Silverio, W.: Assessing high altitude glacier thickness, volume and area changes using field, GIS and remote sensing techniques: the case of Nevado Coropuna (Peru), The Cryosphere, 4, 313–323, doi:10.5194/tc-4-313-2010, 2010.

Pellicciotti, F., Stephan, C., Miles, E., Herreid, S., Immerzeel, W. W., and Bolch, T.: Mass-balance changes of the debris-covered glaciers in the Langtang Himal, Nepal, from 1974 to 1999, J. Glaciol., 61, 373–386, 2015.

Pepin, N., Bradley, R. S., Diaz, H. F., Baraer, M., Caceres, E. B., Forsythe, N., Fowler, G., Greenwood, M. Z., Hashmi, X. D., Liu, J. R., Miller, K., Ning, A., Ohmura, E., Palazzi, I., Rangwala, W., Schöner, I., Seversky, M., Shahgedanova, M., Wang, S. N. Williamson, N., and Yang, D. Q.: Elevation-dependent warming in mountain regions of the world, Nature Clim. Change, 5, 424–430, 2015.

Quincey, D. J., Luckman, A., and Benn, D.: Quantification of Everest region glacier velocities between 1992 and 2002, using satellite radar interferometry and feature tracking, J. Glaciol., 55, 596–606, 2009.

Racoviteanu, A. E., Williams, M. W., and Barry, R. G.: Optical remote sensing of glacier characteristics: A review with focus on the Himalaya, Sensors, 8, 3355–3383, 2008.

Ragettli, S., Bolch, T., and Pellicciotti, F.: Heterogeneous glacier thinning patterns over the last 40 years in Langtang Himal, Nepal, The Cryosphere, 10, 2075–2097, doi:10.5194/tc-10-2075-2016, 2016.

Reynolds, J. M.: Glacial hazard assessment at Tsho Rolpa, Rolwaling, Central Nepal, Q. J. Eng. Geol. Hydroge., 32, 209–214, 1999.

Rignot, E., Echelmeyer, K., and Krabill, W.: Penetration depth of interferometric synthetic-aperture radar signals in snow and ice, Geophys. Res. Lett., 28, 3501–3504, 2001.

Rounce, D. R. and McKinney, D. C.: Debris thickness of glaciers in the Everest area (Nepal Himalaya) derived from satellite imagery using a nonlinear energy balance model, The Cryosphere, 8, 1317–1329, doi:10.5194/tc-8-1317-2014, 2014.

Rowan, A. V., Egholm, D. L., Quincey, D. J., and Glasser, N. F.: Modelling the feedbacks between mass balance, ice flow and debris transport to predict the response to climate change of debris-covered glaciers in the Himalaya, Earth Planet. Sc. Lett., 430, 427–438, 2015.

Sakai, A., Chikita, K., and Yamada, T.: Expansion of a moraine-dammed glacial lake, Tsho Rolpa, in Rolwaling Himal, Nepal Himalaya, Limnol. Oceanogr., 45, 1401–1408, 2000.

Sakai, A., Nuimura, T., Fujita, K., Takenaka, S., Nagai, H., and Lamsal, D.: Climate regime of Asian glaciers revealed by GAMDAM glacier inventory, The Cryosphere, 9, 865–880, doi:10.5194/tc-9-865-2015, 2015.

Salerno, F., Thakuri, S., D'Agata, C., Smiraglia, C., Manfredi, E. C., Viviano, G., and Tartari, G.: Glacial lake distribution in the Mount Everest Region: Uncertainty of measurement and conditions of formation, Global Planet. Change, 92–93, 30–39, 2012.

Salerno, F., Guyennon, N., Thakuri, S., Viviano, G., Romano, E., Vuillermoz, E., Cristofanelli, P., Stocchi, P., Agrillo, G., Ma, Y., and Tartari, G.: Weak precipitation, warm winters and springs impact glaciers of south slopes of Mt. Everest (central Himalaya) in the last 2 decades (1994–2013), The Cryosphere, 9, 1229–1247, doi:10.5194/tc-9-1229-2015, 2015.

Scherler, D., Leprince, S., and Strecker, M. R.: Glacier-surface velocities in alpine terrain from optical satellite imagery – Accuracy improvement and quality assessment, Remote Sens. Environ., 112, 3806–3819, 2008.

Scherler, D., Bookhagen, B., and Strecker, M. R.: Hillslope-glacier coupling: The interplay of topography and glacial dynamics in High Asia, J. Geophys. Res., 116, F02019, doi:10.1029/2010JF001751, 2011.

Shea, J. M., Immerzeel, W. W., Wagnon, P., Vincent, C., and Bajracharya, S.: Modelling glacier change in the Everest region, Nepal Himalaya, The Cryosphere, 9, 1105–1128, doi:10.5194/tc-9-1105-2015, 2015.

Shrestha, A. B., Wake, C. P., Mayewski, P. A., and Dibb, J. E.: Maximum temperature trends in the Himalaya and its vicinity: An analysis based on temperature records from Nepal for the period 1971–94, J. Climate, 12, 2775–2786, 1999.

Somos-Valenzuela, M. A., McKinney, D. C., Rounce, D. R., and Byers, A. C.: Changes in Imja Tsho in the Mount Everest region of Nepal, The Cryosphere, 8, 1661–1671, doi:10.5194/tc-8-1661-2014, 2014.

Storey, J., Choate, M., and Lee, K.: Landsat 8 Operational Land Imager On-Orbit Geometric Calibration and Performance, Remote Sens., 6, 11127–11152, 2014.

Thakuri, A., Salerno, F., Bolch, T., Guyennon, N., and Tartari, G.: Factors controlling the accelerated expansion of Imja Lake, Mount Everest region, Nepal, Ann. Glaciol., 57, 245–257, doi:10.3189/2016AoG71A063, 2016.

Thakuri, S., Salerno, F., Smiraglia, C., Bolch, T., D'Agata, C., Viviano, G., and Tartari, G.: Tracing glacier changes since the 1960s on the south slope of Mt. Everest (central Southern Himalaya) using optical satellite imagery, The Cryosphere, 8, 1297–1315, doi:10.5194/tc-8-1297-2014, 2014.

Thompson, S. S., Benn, D. I., Dennis, K., and Luckman, A.: A rapidly growing moraine-dammed glacial lake on Ngozumpa Glacier, Nepal, Geomorphology, 145, 1–11, doi:10.1016/j.geomorph.2011.08.015, 2012.

USGS: Shuttle Radar Topography Mission (SRTM) 1 Arc-Second Global, available at: https://lta.cr.usgs.gov/SRTM1Arc, last access: 8 March 2016.

Vuichard, D. and Zimmerman, M.: The 1985 Catastrophic Drainage of a Moraine-Dammed Lake, Khumbu Himal, Nepal: Cause and Consequences, Mt. Res. Dev., 7, 91–110, 1987.

Wagnon, P., Vincent, C., Arnaud, Y., Berthier, E., Vuillermoz, E., Gruber, S., Ménégoz, M., Gilbert, A., Dumont, M., Shea, J. M., Stumm, D., and Pokhrel, B. K.: Seasonal and annual mass balances of Mera and Pokalde glaciers (Nepal Himalaya) since 2007, The Cryosphere, 7, 1769–1786, doi:10.5194/tc-7-1769-2013, 2013.

Wang, D. and Kääb, A.: Modeling glacier elevation changes from DEM time series, Remote Sens., 7, 10117–10142, 2015.

Watson, C. S., Quincey, D. J, Carrivick, J. L., and Smith, M. W.: The dynamics of supraglacial ponds in the Everest region, central Himalaya, Global Planet. Change, 142, 14–27, 2016.

Yang, X., Zhang, T., Qin, D., Kang, S., and Qin, X.: Characteristics and Changes in Air Temperature and Glacier's Response on the North Slope of Mt. Qomolangma (Mt. Everest), Arct. Antarct. Alp. Res., 43, 147–160, 2011.

Ye, Q., Kang, S., Chen, F., and Wang, J.: Monitoring glacier variations on Geladandong mountain, central Tibetan Plateau, from 1969 to 2002 using remote-sensing and GIS technologies, J. Glaciol., 52, 537–545, 2006.

Ye, Q., Bolch, T., Naruse, R., Wang, Y., Zong, J., Wang, Z., Zhao, R., Yang, D., and Kang, S.: Glacier mass changes in Rongbuk catchment on Mt. Qomolangma from 1974 to 2006 based on topographic maps and ALOS PRISM data, J. Hydrol., 530, 273–280, 2015.

Zhao, L., Ding, R., and Moore, J. C.: The High Mountain Asia glacier contribution to sea-level rise from 2000 to 2050, Ann. Glaciol., 57, 223–231, doi:10.3189/2016AoG71A049, 2016.